Schweizerische Eidgenossenschaft
Confédération suisse
Confederazione Svizzera
Confederaziun svizra

Federal Department of the Environment,
Transport, Energy and Communications DETEC

Swiss Federal Office of Energy
Energy Research and Cleantech

Final report from 13 March 2025

MoCool

Occupant-centric, **mo**bile, radiant panel **cool**ing for increasing summer comfort in offices

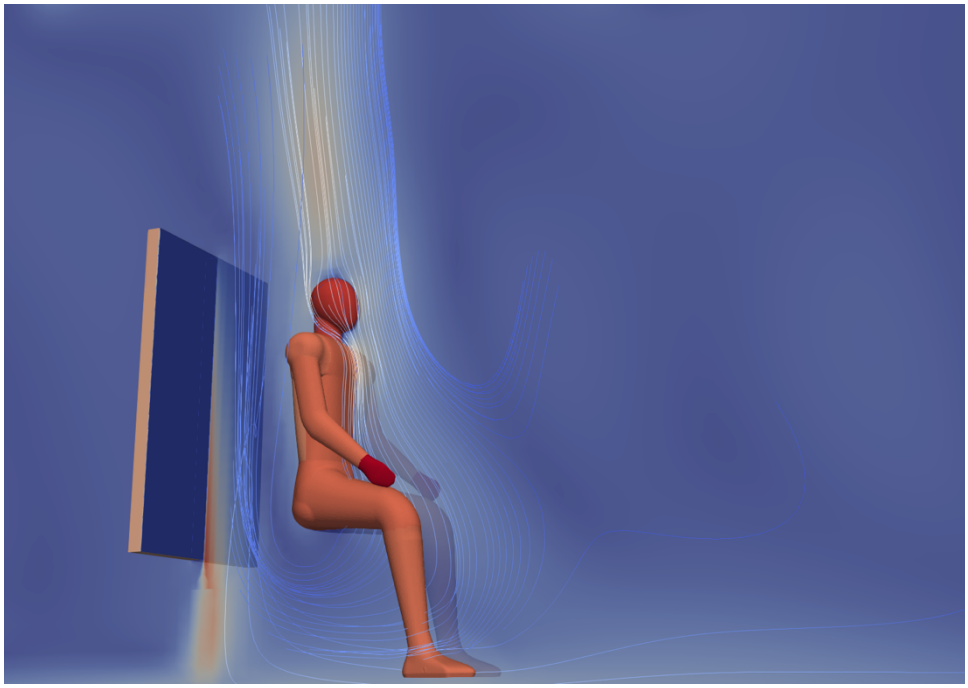

Source: © IBP - ZHAW, 2025

Publisher:
Swiss Federal Office of Energy SFOE
Energy Research and Cleantech
CH-3003 Berne
www.energy-research.ch

Subsidy recipients:
ZHAW Centre for Building Technologies and Processes ZBP
Tössfeldstrasse 11, 8401 Winterthur
https://www.zhaw.ch/de/archbau/institute/zbp

Autors:
Juan Mahecha, ZHAW ZBP, mahe@zhaw.ch
Luca Baldini, ZHAW ZBP, luca.baldini@zhaw.ch

SFOE project coordinators:
Martin Ménard, menard@lowtechlab.ch
Nadège Vetterli, nadege.vetterli@anex.ch

SFOE contract number: SI/502568-01

Summary

This project proposes a novel mobile panel cooling solution for buildings in response to the increasing demand for space cooling. By using phase change materials to store heat, the cooling panels are not permanently installed but can be moved freely around the room and only used when needed. The project determined to what extent thermal comfort can be achieved with a local and flexible cooling solution based on radiant cooling and what potential energy savings can be expected when using such a targeted and local cooling solution compared to room air cooling with conventional HVAC systems. Research work included different levels of simulations along with physical prototyping and an experimental validation. By coupling computational fluid dynamics simulation with thermoregulation models the thermal heat balance of an individual subject could be studied in detail, allowing to quantify the effect local radiant cooling panel take on the thermal comfort. The results clearly show that under the chosen design conditions, up to moderately high room temperatures of 28°C thermal comfort can be fully restored using local panel cooling while up to 30°C thermal comfort can be significantly improved. Further, the analysis revealed that for office spaces with a moderate overheating and with less than 40% predicted percentage of dissatisfied occupants local panel cooling represents a feasible cooling solution, providing potential savings in energy consumption and embodied emissions by a factor of 2-6 when compared to a conventional cooling system. Finally, the preliminary experimental testing was able to qualitatively confirm the positive cooling effect of the local panels as predicted by the simulations but further tests will be required in future to better understand its limitations.

Zusammenfassung

In diesem Projekt wird eine neuartige mobile Paneelkühllösung für Gebäude vorgeschlagen, um dem steigenden Bedarf an Raumkühlung zu begegnen. Durch die Verwendung von Phasenwechselmaterialien zur Speicherung von Wärme sind die Kühlpaneele nicht fest installiert, sondern können frei im Raum bewegt und nur bei Bedarf genutzt werden. Im Rahmen des Projekts wurde ermittelt, inwieweit mit einer lokalen und flexiblen Kühlungslösung auf der Grundlage von Strahlungskühlung thermischer Komfort erreicht werden kann und welches Energieeinsparungspotenzial bei Verwendung einer solchen gezielten und lokalen Kühlungslösung im Vergleich zur Raumluftkühlung mit herkömmlichen HLK-Systemen zu erwarten ist. Die Forschungsarbeiten umfassten verschiedene Simulationen sowie die Erstellung von physikalischen Prototypen und eine experimentelle Validierung. Durch die Kopplung von numerischen Strömungssimulationen mit Thermoregulationsmodellen konnte der Wärmehaushalt einer einzelnen Person im Detail untersucht werden, so dass die Auswirkung lokaler Strahlungskühlpaneele auf den thermischen Komfort quantifiziert werden konnte. Die Ergebnisse zeigen deutlich, dass unter den gewählten Auslegungsbedingungen bis zu mässig hohen Raumtemperaturen von 28°C die thermische Behaglichkeit durch die lokale Paneelkühlung vollständig wiederhergestellt werden kann, während die thermische Behaglichkeit bei bis zu 30°C deutlich verbessert werden kann. Darüber hinaus ergab die Analyse, dass für Büroräume mit mässiger Überhitzung und einem prognostizierten Prozentsatz unzufriedener Nutzer von weniger als 40 % die lokale Flächenkühlung eine praktikable Kühllösung darstellt, die im Vergleich zu einem konventionellen Kühlsystem Einsparungen beim Energieverbrauch und den grauen Emissionen um den Faktor 2-6 ermöglicht. Schliesslich konnten die vorläufigen experimentellen Tests den von den Simulationen vorhergesagten positiven Kühleffekt der lokalen Paneelkühlung qualitativ bestätigen, doch sind in Zukunft weitere Tests erforderlich, um dessen Einsatzgrenzen besser zu verstehen.

Résumé

Ce projet propose une nouvelle solution de refroidissement par panneaux mobiles pour les bâtiments en réponse à la demande croissante de refroidissement des espaces. En utilisant des matériaux à changement de phase pour le stockage de l'énergie thermique, les panneaux de refroidissement ne sont pas des installations fixes mais peuvent être déplacés librement dans l'espace et utilisés uniquement à la demande. Le projet a permis de déterminer dans quelle mesure le confort thermique peut être atteint avec une solution de refroidissement locale et flexible basée sur le refroidissement par rayonnement et quelles économies d'énergie potentielles peuvent être attendues lors de l'utilisation d'une telle solution de refroidissement ciblée et locale par rapport au refroidissement de l'air ambiant avec des systèmes CVC conventionnels. Le travail de recherche comprenait différents niveaux de simulation ainsi qu'un prototypage physique et une validation expérimentale. En associant la simulation de la dynamique des fluides à des modèles de thermorégulation, le bilan thermique d'un sujet individuel a pu être étudié en détail, ce qui a permis de quantifier l'effet d'un panneau de refroidissement par rayonnement sur le confort thermique. Les résultats montrent clairement que dans les conditions de conception choisies, jusqu'à des températures modérément élevées de 28°C, le confort thermique peut être entièrement rétabli en utilisant un panneau de refroidissement local, tandis que jusqu'à 30°C, le confort thermique peut être amélioré de manière significative. En outre, l'analyse a révélé que pour les espaces de bureaux avec une surchauffe modérée et avec un pourcentage prévu de moins de 40% d'occupants insatisfaits, le refroidissement local par panneaux représente une solution de refroidissement réalisable, offrant des économies potentielles en termes de consommation d'énergie et d'émissions grises d'un facteur de 2 à 6 par rapport à un système de refroidissement conventionnel. Enfin, les essais expérimentaux préliminaires ont permis de confirmer qualitativement l'effet de refroidissement positif des panneaux locaux prévu par les simulations, mais d'autres essais seront nécessaires à l'avenir pour mieux comprendre ses limites.

Main findings («Take-Home Messages»)

- Occupant-centric, physics-based comfort metrics introduced in this project enhance understanding and the analysis of thermal comfort. They quantify the impact of indoor environments directly on the human heat balance.
- Simulations show that PRCS are capable of restoring comfort up to room temperatures of 28 °C and lead to noticeable comfort improvement up to temperatures of 30°C. At higher temperatures heat dissipation due to sweating cannot be avoided but is reduced.
- PCRS represents a minimal and tailored cooling solution to mitigate individual discomfort with significant potential in energy and embodied emission savings of a factor of 2-6. The savings are the bigger the lower the occupancy and simultaneity levels.
- Experiments conducted confirm the effect and comfort improvements but show a need for further and more detailed experimental campaigns.

Contents

List of figures

List of tables

List of abbreviations

SFOE	Swiss Federal Office of Energy
AC	Air Conditioning
AMV	Actual Mean Vote
CFD	Computational Fluid Dynamics
CHT	Conjugated Heat Transfer
CSM	Compact Storage Modules
ET	Equivalent Temperature
HVAC	Heating, Ventilation, and Air Conditioning System
JOS	Joint system thermoregulation model
KPI	Key Performance Indicator
LTC	Local Thermal Comfort
LTS	Local Thermal Sensation
MET	Metabolic rate
MRT	Mean Radiant Temperature
PCM	Phase change material
PRCS	Personal Radiant Cooling System
PMV	Predicted Mean Vote
PPD	Predicted Percentage of Dissatisfied index
RH	Relative Humidity
RHD	Reference Heat Deviation
RHDT	Reference Heat Deviation Temperature
SET	Standard Equivalent Temperature
TCV	Thermal Comfort Vote
TS	Thermal Sensation
TSV	Thermal Sensation Vote

1 Introduction

1.1 Context and motivation

Ongoing climate change, continuing urbanization, and increasing comfort expectations are drivers towards increased cooling demand in buildings, even in moderate climates such as Switzerland [1] [2].

A particular challenge regarding space cooling is given by the fact that Switzerland, like many other countries, has a large existing building stock and a low renovation rate of about 1%. As a consequence, a potential switching from only heating to integral heating and cooling systems will take very long and thus not be able to address the quickly growing space cooling demand. Better retrofit solutions other than standard, inefficient RAC units are needed, allowing to implement cooling with an acceptable effort and investment.

Traditional HVAC systems are designed to condition the entire building volume to ensure thermal comfort. However, these systems neglect the occupants' diversity, individual needs, and preferences, especially in large spaces such as open-floor office configurations. Besides, energy efficiency can be poor when the entire space is conditioned while occupancy levels are low.

As a response to the challenges mentioned, this project proposes a novel cooling approach for office buildings based on an efficient, renewable cold generation and mobile cold storage and radiant emission system. This system eliminates the need for complicated and costly integration of cold distribution and steady emission systems in the office space.

1.2 Project objectives

This study aims to understand the potential of decentralised, occupant-centric radiant cooling panels to improve thermal comfort in an office building under summer cooling conditions. To this end, the project aims to study thermal comfort using a novel simulation framework, identify design parameters for effective panel cooling, virtual and real prototyping of a mobile radiant cooling panel, experimental evaluation using surface temperature measurements and user surveys/feedback.

Specific goals are:

- Identification of comfort gain achieved, applying mobile, radiant panel cooling for different use cases and scenarios
- Identification of potential energy (operative and embodied) and cost savings compared to defined benchmark cooling systems
- Prototypical implementation of a mobile, radiant cooling panel
- Verification of performance and enhanced occupants' comfort by experiments with panel prototype using measurements (infrared camera) and real user feedback

Overall, the feasibility of local radiant panel cooling, in terms of achieved comfort gain, energy-saving potential, usability and economic viability, will be assessed. Thereby, the following **questions** shall be answered by this research:

- What are realistic use cases for deploying mobile, radiant cooling panels?
- Under what circumstances/scenarios (building type, window fraction/location, room partitioning, workspace configuration, occupancy pattern, internal loads, etc.) can local radiant panel cooling improve individual thermal comfort?
- What are the relevant design parameters (panel configuration, active area, surface temperature, etc.) and what are the thresholds for these parameter values to allow for effective comfort improvement? How can design requirements be translated into a cost-effective mobile panel

solution? Are results achieved using simulations consistent with experimental results and individual user feedback?

- What comfort gains and energy savings are achieved compared to different well-established benchmark solutions?

2 Definitions, concepts, system design and use cases

This section analyses state-of-the-art occupant-centric radiant cooling strategies to establish a foundation for designing and evaluating the proposed mobile and occupant-centric radiant cooling system. It complements the findings with a workshop with the industrial partner, Witzig - The Office Company, where envisioned opportunities and challenges of deploying the solution in real office environments are discussed. Finally, it presents the use cases and functional requirements identified, discusses the foresaw cold generation methods, and concludes with a parameter tree that serves as input for the design process.

2.1 Literature review[1]

Zhang et al. [4] have reviewed the literature concerning personalised radiant cooling and heating systems. Regarding cooling applications, they have documented systems that focus on influencing the micro-environment in the proximity of the occupant using thermally activated furniture, vertical panels, and ceiling panels. Further, the systems have been tested as standalone [5], [6], [7] or combined with personal fans [8], HVAC systems [9], [10], [11], [12], [13], [14], radiant ceilings [5], [15], and diffuse ventilation [16]. Table 1 summarises the personalised radiant cooling systems (PRCS) studied in the literature, the methods implemented, and the parameters and comfort metrics evaluated.

Most studies have been conducted using experimental methods in controlled environments [5], [6], [7], [8], [9], [10], [15], [16]. While some studies have used thermal manikins to simulate the thermal load of the occupants, i.e., using a fixed temperature [16] or heat flux [10], and measuring the indoor environmental quality, others have used human subjects and questionnaires to assess the impact on thermal comfort [6], [7], [8], [9], [15]. In addition, some studies have implemented computational fluid dynamics (CFD) models to evaluate the performance of the PRCS numerically [11], [12], [13], [14].

In detail, [6] pointed out that user-centric radiant cooling panels are a flexible, efficient and local way to provide thermal comfort, especially in open-plan offices. They highlighted that typical limitations due to water vapour condensation in ceiling-mounted systems could be relaxed using a vertical panel solution. A case study was performed with a single, laterally placed vertical cooling panel. They found that comfort/thermal sensation could be improved mostly for moderate air temperature (28°C) and relatively low panel surface temperature (10°C), though allowing for condensation. The limited angle factor could explain the minute comfort gain for more extreme ambient conditions (30°C). Moreover, [11] studied the performance of a personalised cooling radiant cubicle (PCRC) combined with a conventional HVAC system. Using a novel numerical model based on CFD and mathematical formulations, they demonstrated the PCRC maintained a comfortable personal thermal environment in the target zone, reduced the thermal asymmetry, and improved the corresponding predicted percentage of dissatisfied (PPD) index. Further, the PCRC allowed increasing the thermostat setpoint of the conditioned air by the HVAC. Thus, it reduced the HVAC cooling energy by 18%. After, [17] included an optimisation study using artificial neural networks (ANN) trained with the CFD model developed in [11]. Considering the HVAC supply temperature, the panel inlet water temperature, and the water mass flow rate,

[1] A summary of this section has been presented in [3]

the annual energy consumption and the predicted percentage of dissatisfied individuals were optimised.

[18] presented a preliminary, experimental comfort study for thermoelectrically cooled surfaces for radiant cooling. The experimental setup consisted of a panel placed laterally to an office desk. The room air was controlled to remain between 27 and 29°C. Thermal comfort was evaluated through questionnaires, asking for metrics such as overall thermal sensation and comfort. The cooling panel operation showed a slight improvement in both metrics. Similarly, [19] studied a thermoelectric cooling panel using a climate chamber, a thermal manikin and virtual reality (VR). They found that the thermoelectric panel had a more significant effect at higher room temperatures, showing a reduction of local skin temperature by up to 0.5K. In [9], a radiant cooling desk was assessed through experiments, comparing its performance to a similar office desk without cooling. The cooling desk consisted of panels surrounding the desk laterally and in the front. The experiments were carried out cooling only the panel in the front and the actual desk. Room air temperature was controlled to 28, 30 and 32 °C with corresponding cooled desk surface temperatures of 22.8, 23.9 and 25.5 °C. The thermal comfort was evaluated through questionnaires, asking for comfort metrics such as overall thermal sensation and thermal comfort. Results showed that the radiant cooling desk reduced warm sensation and improved overall thermal comfort, even at high room air temperatures of 32°C. The study identifies a strong effect of locally cooled body parts using direct contact with the cooled desk surface.

In [20] an activated furniture cooling system was studied employing CFD modelling. The setup consisted of a vertical radiant panel in front of the user sitting at a desk. A thermal mannikin is modelled with a detailed analysis of the resulting skin temperature for different body parts. From this and other variables provided by the CFD simulation, the thermal comfort was assessed by calculating the PMV. The analysis showed that PMV votes were significantly lower at moderate room air temperatures (26°C) compared to elevated temperatures of 28 or 30°C. However, the decrease in PMV value was similar for all conditions (towards a more neutral thermal sensation) with the increasing temperature difference between room air and panel surface temperature (restricted to max. 8K). Again, this study states the feasibility of a user-centric radiant cooling approach (without conditioning the surrounding space), highlighting the limited impact due to the relatively small angle factor in the case of applying it only to the front desk panel.

Finally, [5] experimentally investigated a personalised radiant cooling system in an office cubicle. The U-shaped cubicle featured an activated surface area of 4.32 m (12 radiant cooling panels of 0.6 x 0.6 m). Air and mean radiant temperatures are recorded, and operative and standard effective temperatures (SET) are calculated. SET is used as the primary criterion for comfort evaluation. Experiments showed that the personalised radiant cooling solution could keep SET within a comfortable range of 23-26°C for supply water temperatures of 15-19°C. In contrast, the radiant cooling ceiling system maintained comparable comfort only for the minimum supply temperature of 15°C. For this reason, the personalised cooling system could be operated with higher supply temperatures than the ceiling system, leading to an estimated 60% reduction in chiller electric energy demand.

Table 1. Literature on personalised radiant cooling systems (Adapted and extended from [4]).

Ref.	PRCS	HVAC / Room conditions	Methodology	KPI	Highlights
[5]	Radiant cubicle: • 12 panels: 0.6m x 0.6m • Supply water: 15°C – 21°C • Target: Micro-environment	Radiant Ceiling • Supply water: 15°C – 21°C • Air temperature: 27.7°C – 30.8°C • RH 40%	Experimental Study: Indoor environmental parameters	• SET: Standard effective temperature • Response Time	Energy savings of around 60% with the personal system alone and 23% in combination with the ceiling system

Ref.	PRCS	HVAC / Room conditions	Methodology	KPI	Highlights
[8]	Radiant workstation: • Radiant front and horizontal (desk) panels • Surface temperature 24°C • Target: Upper body	AC and Personal fan • Air temperature: 27.7°C – 30.8°C • RH 80%	Experimental Study: Human subjects	• TS: Overall/Local thermal sensation	The combination of radiant cooling workstation and desktop fan brings the thermal sensation close to the neutral condition with air temperatures up to 30°C
[9]	Radiant workstation: • Radiant front and horizontal (desk) panels • Surface temperature 22.8 – 25.5°C • Target: Upper body	AC • Air temperature: 28°C – 32°C • RH 60%	Experimental Study: Human Subjects	• O/LTS: Overall/Local thermal sensation • O/LTC: Overall/Local thermal comfort • Air movement sensation and preference	The system reduced warm sensation and improved thermal comfort. More than 80% of the subjects felt acceptable at 32°C. Highlighted the importance of conducting the experiments considering additional parameters, e.g., air velocity
[10]	Thermally activated furniture • Radiant front and lateral panels: 1.2m x 1.2m • Surface temperature 18 – 30°C • Target: Micro-environment	HVAC • Air temperature: 26°C – 30°C • RH 50%	Experimental Study: Thermal manne-quin	• Skin temperature • Body heat flux • PMV	Under a fixed metabolic rate of 1.1MET, using the radiant panels, acceptable conditions are achieved for an air temperature between 26°C and 28°C. At 30°C, there is an improvement, but thermal comfort is not achieved.
[16]	Radiant ceiling panel: • Two radiant panels above the workstations • Surface temperature: 15°C • Target: Micro-environment	Low-velocity air units: • Air temperature: 15°C • RH 50%	Experimental Study: Indoor environmental parameters	• Air velocity and temperature stratification • Draught rate • Air change index	The low-velocity radiant system is compared to a diffuse ceiling ventilation system. The former has a smaller vertical temperature gradient and generates a better micro-environment. Further, the radiant system meets better thermal comfort ranges.
	Radiant cooling panels: • One vertical, lateral radiant panel 1.26m x 1.25m • Surface temperature: 10°C – 28°C	Humidifier and Heaters • Air temperature: 28°C - 30°C • RH 40%	Experimental Study: Indoor environmental parameters & Human subjects	• Temperature and velocity profiles • Thermal Sensation Vote • Thermal Acceptability Vote • Thermal Comfort Vote • Air Quality • Air movement	The air velocity is high only at distances below 5cm; thereby, there is no risk of draught or discomfort due to turbulence close to the occupant. Despite low panel temperatures, the risk of condensation is not high under the tested conditions. Thermal sensation significantly improves at an air temperature of 28°C. At 30°C, the improvement is limited. The participants' thermal sensation and calculated PMV diverge at 28°C.
[11], [12]	Radiant cooling cubicle: • Front and lateral panels at desk level: 6m^2 • Inlet water temperature: 12-17°C • Target: Upper body	AC: • Air temperature: 14-18°C • RH 50%	Numerical Simulation: • CFD – Thermal manikin with a constant heat flux (MET)	• PMV • PPD	Air velocity and temperature around the occupant are calculated from the CFD simulation 1cm away from the manikin. The study finds it is possible to increase the cooling setpoint (18°C) using the radiant panels. The cooling load is reduced by 50% compared to a case without radiant panels and lower cooling setpoint (14°C)

Ref.	PRCS	HVAC / Room conditions	Methodology	KPI	Highlights
[15]	Personal radiant cubicle: • Front and lateral radiant panels • Supply water temperature: 15°C-21°C • Target: Micro-environment	AC or Radiant cooling ceiling • Ambient temperature: 31°C – 37°C • RH: 29% - 55% • Air velocity: 0.1m/s – 0.2m/s	Experimental study: • Indoor environmental parameters • Human Subjects	• SET • Thermal sensation	The personal system provides adequate cooling and thermal comfort around the occupant with a water supply between 15°C and 19°C. In combination with the radiant ceiling system, higher water supply temperatures of 17°C-21°C can be set.
[13], [14]	Personal radiant cooling panel: • Front radiant panels at desk level • Surface temperature: 5° - 15°C • Target: Upper body	AC: • Ambient temperature: 25.9°C-27.5°C • RH: 60% • Air velocity: 0.15m/s	Numerical Simulation: • CFD – Thermal manikin with a constant heat flux (MET) Experimental study for validation: Thermal manikin	• Percentage dissatisfied (PD) with radiant temperature asymmetry and vertical air temperature difference	A parametric sweep assesses thermal comfort using PD with thermal asymmetry and air temperature stratification. Thermal comfort is achieved using the radiant panels under tested conditions. A layer of air is integrated into the system to prevent condensation. Mean radiant temperature calculated at a reference point. Implementing the radiant cooling system allowed for an increase of 1.6°C supply air temperature and 0.54°C the indoor air temperature, achieving the same operative temperature as the benchmark (AC).

The following central observations can be underlined: PRCS can achieve comfort levels at low to moderate indoor air temperatures (~ 26-28 °C); improvements are perceived at higher temperatures, but PRCS can not reach the desired comfort levels as standalone systems. PRCS can be combined with other systems, such as personal fans and radiant ceilings, to provide thermal comfort in these cases. Regarding the indoor environment, it has been shown that with the PRCS, the risk of draught and high air velocities around the occupant is low [6], [7]. Finally, important questions are raised about the validity of using traditional comfort metrics such as PMV when using radiant systems. In particular, [7] showed a disagreement between the thermal sensation and PMV at non-extreme indoor air temperatures, i.e., 28°C.

Notwithstanding the reviewed studies showing a general positive influence of PRCS on thermal comfort, indoor environmental quality, and energy efficiency, some limitations were identified. It has been highlighted that radiant systems cannot control the latent loads; thus, systems such as dehumidifiers might be required, especially in tropical climates. Further, there is a risk of condensation in low-temperature radiant cooling systems. While some studies have addressed the issue by maintaining the system temperature above the dew point to prevent vapour condensation or integrating collection trays to collect condensed water [7], recently, an integrated air layer separated by a membrane has proven to be efficient in avoiding this problem while lowering the system temperature below the dew point [13], [14]. This alternative has been explored under outdoor conditions in tropical climates, and promising results have been shown [21].

2.2 Workshop: Opportunities and challenges

In the following, an overview of the 1st workshop with the implementation partner is given, providing the list of people who attended, the workshop programme and a summary of the outcomes.

Participants:

<u>Witzig:</u>

- Glarner Christian (Project lead Witzig, product management)

- Weber Daniel (Strategic Sales)
- Schwyn Roger (Consulting / Sales)
- Kessi Renato (Planning and Design)
- Hagander Ann-Sophie (Interior Design)
- Peter Manuela ("New Work Academy" / New Office and Work concepts)

ZHAW:

- Baldini Luca (Project lead / Research)
- Mahecha Juan (Research)
- Ebnöther Yves (Industrial Design)

The workshop started with an introduction to radiant cooling and the specific project goal of exploring the potential of a mobile cooling solution for office spaces. After, two brainstorming and discussion sessions were held to establish the boundary conditions for a mobile panel solution and explore potential design concepts. Specific points raised were:

- Discussion of room concepts/design options (new possibilities with mobile - Installation-bound cooling panels vs. mobile cooling panels)
- Identification of suitable use cases and definition of 2-3 specific cases
- Definition of occupancy scenarios/use profile
- Discussion of handling/usability: requirements, limitations
- Combining Witzig's concepts/solutions with the panel cooling concept
- Co-creation process for defining new solutions for integrated mobile panel cooling

In **session 1**, the specific task was to test the project idea with the implementation partner and ask the participants about potential opportunities, challenges and risks they anticipate. The participants were asked the following questions:

- Why could the concept work? Why could it fail?
- Do you anticipate opportunities or solutions?
- In which scenarios could it work? In which scenarios might not be feasible?

The feedback was written down on post-its that were clustered and consolidated on a board (Figure 1).

The main points identified in this session were:

Table 2: Inputs from workshop participants regarding potential opportunities, challenges and risks.

Opportunities	**Challenges**	**Risks**
- Multi-functionality: shading + cooling + whiteboard + privacy panel + acoustic absorber + …	- Spatial arrangement, focusing of cooling effect / view factor	- Minimal / insufficient comfort gain
- Personalized climate control	- Handling: people forget to recharge	- Discomfort / temperature asymmetry
- Possibility for integration in clothing	- Required infrastructure for charging	- Complicated handling
- Cooling and/or heating possible		- High maintenance

- Applicable for flexible/changing room concepts, for individual work space or meeting rooms (room in room concept with no cooling installed)

- Integration with rest of HVAC system
- Cost of decentralized cooling solution
- …

- Sustainability of PCM
- …

Figure 1: Feedback regarding opportunities, challenges and risks collected and clustered on a board during session 1 of the workshop

In **session 2** of the workshop, the goal was to understand possible application scenarios better or features a mobile cooling solution should have to provide a benefit. The specific questions asked in this context were:

- Could you envision an ideal prototype and an ideal use scenario?
- Where can the solution be used?
- What else could the device do? What shouldn't the device do?
- Foldable/mountable/standing? Dimensions?
- Existing products/functions that can be integrated/adapted/converted?
- Thoughts on charging station/process

These questions were discussed in two separate groups and documented on whiteboards as shown in Figure 2.

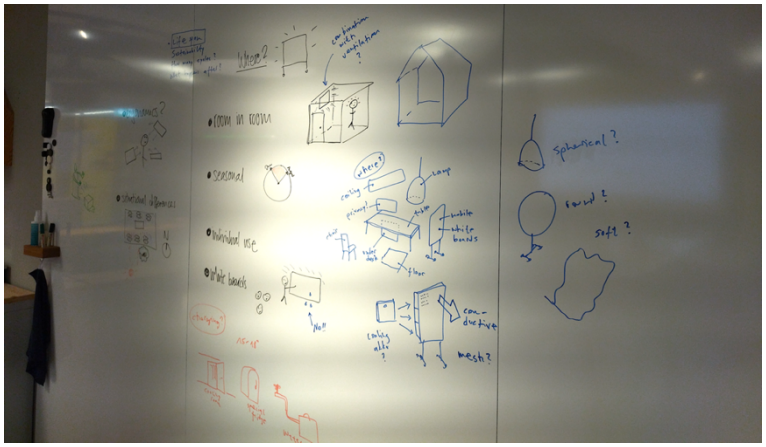

Figure 2: Collection of ideas of one group in session 2.

Session two revealed the following ideas:

- Application in meeting rooms/room-in-room concepts, individual use (more or less, as desired), in open floor offices, in rooms that are/have to be flexible/dynamically reconfigured
- Panel design/integration in mobile whiteboards (active use in summer or passive use in winter), privacy panels, chairs, tables, under the desks, at the ceiling, or on the floor
- Charging options: Cooling room to fit the panels, special fridge to charge the phase change material (PCM) modules, connection to a cold-water loop

In summary, the workshop gave some hints for applying the mobile cooling panels in an office environment. Most often mentioned were either i) the individual cooling or ii) the cooling in a meeting setting, especially in a room-in-room concept where no additional cooling is available.

For the integration, the whiteboard and privacy panel were most often mentioned. The system would be directly mounted in front of the table to separate two opposite workspaces. Multi-functionality was also mentioned in the context of shading/glare protection and acoustic absorption.

Three charging options were discussed (listed above), each impacting space requirement, handling, and panel design differently.

This first workshop was exploratory and provided little to no information on the cooling features of this radiant panel concept. Thus, which of the ideas raised during the workshop are feasible or compatible can only be understood at a later stage when the panel cooling is better characterised. This is the task of WP2, and the insights from the work in WP2 will also build the basis for a second workshop with the business partner Witzig.

2.3 Use cases, functional requirements and conceptual design

Results from the literature review and the workshop findings are synthesised to define the application scenarios and the envisioned functional requirements of the mobile and occupant-centric radiant cooling solution.

The mobile, radiant cooling panel is envisioned as a flexible alternative cooling solution to locally and individually increase thermal comfort in unconditioned or only slightly conditioned office spaces. As such, its main application is seen in large open-plan offices where it is difficult to address individual comfort. Other application cases are considered for room-in-room concepts where cooling is unavailable and its use is irregular. Table 3 summarises the two scenarios and functional requirements defined.

Table 3. Application scenarios and functional requirements (Images generated using Microsoft Copilot).

Scenarios	
Open-plan office layout	**Room-in-room concept**
	
Large working spaces with irregular occupancy patterns, flexible use of personal stations, and where the diversity of occupant's needs and preferences is high.	Room-in-room concepts dedicated for temporal personal use (e.g., focus rooms) or to hold short meetings. In these spaces the available cooling supply is limited or inexisting.
Use	
On-demand use in individual working spaces according to occupant's needs.	On-demand use when cooling loads are high and occupancy periods are long.
Functional requirements	
• The panels are designed to provide daily needs and thus, remaining active for a period between 4 and 6 hours. Enough to ensure thermal comfort during peak occupancy and ambient temperature. • The cooling panels can be recharged during the night. • The cooling panels could integrate multifunctionality: room configurators, whiteboards, sound absorption, privacy panels, etc. • Controlled area of influence: depending on the room temperature, surface temperature, and occupant preferences, the occupant can decide how many panels and where to locate them • The panels should be light, modular, configurable and ideally can be handled by one person, i.e., during charging and transport • The panels need water vapor mitigation measures. This risk can be avoided with high surface temperatures or installing an air bufer layer with a plastic membrane. If condensation is allowed, collection trays or vegetation can be integrated to the design.	

2.3.1 Conceptual design and cold generation methods

The first conceptual design considered for the mobile cooling panel is a multilayer construction, featuring a) an insulation layer on the rear side to avoid undirected convective cooling of the ambient, b) a heat exchanger to allow for heat removal from the PCM to recharge it for later use, c) a PCM layer acting as a cold storage, d) a cover material with good thermal conductivity and absorptance/emissivity. Layers b) and c) could be combined with a heat exchanger immersed in the PCM. However, due to the complexity of manufacturing, uneven temperature distribution, and potential phase separation, this design route is not pursued.

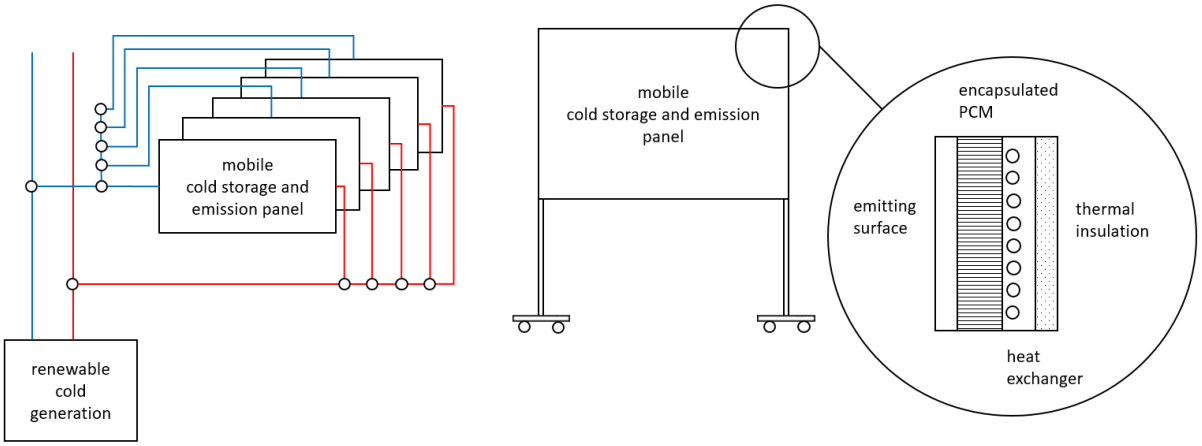

Figure 3. Conceptual design: version 0

Alternatively, a design with macro-encapsulated PCM is followed. In this case, PCM is stored in small, sealed containers (compact storage modules CSM). These CSMs can be readily used in the application, allowing for a modular panel design. Different sizes and thicknesses of such CSMs are available, allowing for different storage capacities to be realised.

The CSMs can be filled with different PCMs characterised by various properties. The phase change temperature, latent heat capacity, and thermal conductivity are key material parameters for the radiant cooling application. The temperature is decisive for the targeted surface temperature of the cooling panel. At the same time, the latent energy storage capacity determines the period during which the panel can be used before recharging is needed. The thermal conductivity is decisive for the charging and discharging of the panel, determining the rate at which heat can be absorbed or removed and influencing the adequate cooling capacity of the panel in operation. There is a large range of suitable PCMs available, comprising both organic and inorganic materials. For their selection, the aforementioned key parameters need to be evaluated, along with the detailed heat absorption and release characteristics. Rather than a singular melting temperature, there is a melting and freezing temperature range; consequently, there is a distributed heat absorption and release, as shown in Figure 4.

Further, the choice of cold generation method constrains the cooling panel design. Three main cold generation concepts are discussed: a) The mobile panel displays an embedded heat exchanger between the insulation layer and the CSMs, which is connected to a chilled water loop in a centralised charging station; b) The entire mobile panel is placed in a cold room (or outdoor space if night ambient temperatures are below the freezing temperature range of the PCM); c) The CSMs are removed from the panel and placed in an industrial fridge. Alternatives a) and b) involve significant interventions to create a centralised charging space, with additional complexity due to the need for recharging the panels horizontally to prevent phase separation and deformation of the CSMs. While these alternatives can be explored in the future, considering this project's scope, they are discarded. Accordingly, the panel design must consider a practical way to remove and place the CSMs horizontally in an industrial fridge.

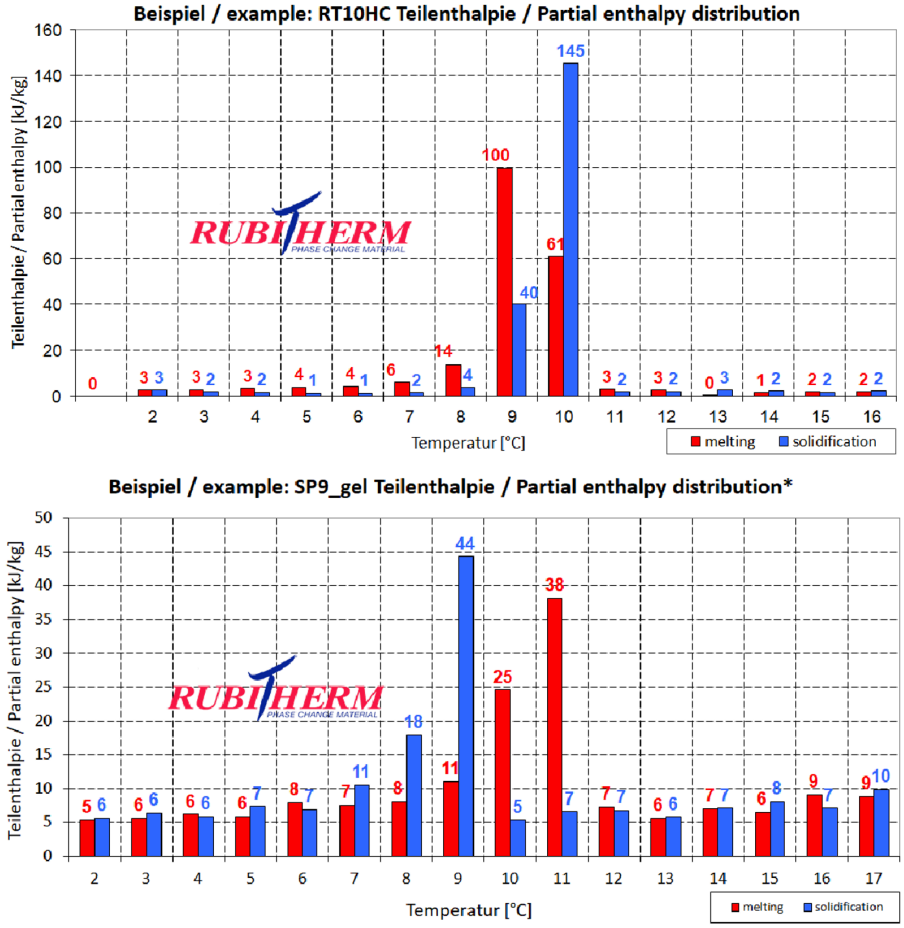

Figure 4. Melting enthalpy distribution for samples of organic (top) and inorganic (bottom) PCMs from Rubitherm (http://www.rubitherm.eu/en).

Considering the previous discussion, the conceptual design of the cooling panel proposed in this project consists of an insulating material in which the CSMs are partially embedded (Figure 5 - Left). In this way, only one side of the CSMs remains active during the discharging process and can be easily removed for the charging process. Alternatively, the whole set of insulating material-CSM could be placed in the fridge at the expense of increasing the charging time (Figure 5 - Right). Furthermore, in a more advanced design stage, depending on the PCM melting temperature range, there is the possibility of adding a frame with a plastic membrane to prevent condensation of the room air, thereby reducing the available panel capacity due to latent loads. Finally, the panel can be mounted on a structure with wheels for easy transport, and the user can choose the number of panels desired and configure their position.

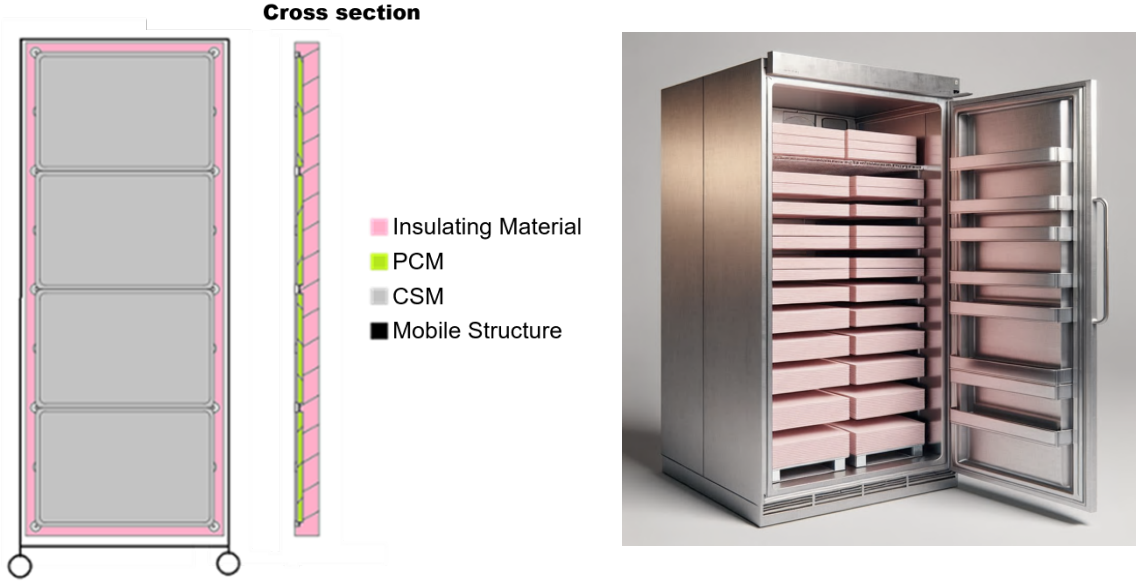

Figure 5. Conceptual design: Cooling panel (Left); Cold generation concept (Right)

2.4 Parameter tree

This section defines the parameter tree and the design of experiments used to evaluate the influence of design parameters and application scenarios on the performance and feasibility of the mobile radiant cooling panel proposed in this project. The evaluation is performed using a simulation-aided design process presented in Sections 3 and 4.

Regarding thermal comfort, the literature highlights (see Section 2.1) that the performance of radiant cooling strategies is influenced by (i) design parameters such as the surface temperature and the configuration of the radiant cooling system, i.e., the active surface area and the view factor relative to the occupant; (ii) indoor environmental parameters such as room air temperature, relative humidity, velocity, and the radiation field; (iii) personal parameters influencing occupants' needs and preferences such as age, gender, activity, position, as well as the physiological and psychological state, and socio-economic background; (iv) contextual parameters such as room layout, furniture, appliances and devices, time of the day, and weather conditions.

Regarding energy performance and energy-saving potential, radiant cooling strategies are influenced by factors such as the building's envelope quality, the size of the conditioned space, ventilation strategies, shading and window operation, occupancy patterns, cooling setpoint preferences, and electrical appliances.

Considering the extensive design and application space, some decisions need to be fixed to reduce the size of the scenarios evaluated. To this end, thermal comfort is evaluated by assuming a fixed relative humidity and air velocity for an occupant with defined personal characteristics, physical activity and clothing. The physiological, psychological and behavioural aspects are considered out of this project's scope. In these cases, the parameters explored are the room temperature, the radiant cooling panels' surface temperature and configuration. This exploration is performed in two stages: the first one considers three room temperatures, i.e., 28, 31.5 and 35°C; three surface temperatures, i.e., 10, 15, and 20°C; four configurations, i.e., back, side, side-back, side-back-side (see Table 4). With a full factorial design, 36 scenarios are analysed. The outcomes of this explorative study are used to refine the design space with three room temperatures, two surface temperatures and three configurations, resulting in 18 scenarios. The results of this second stage are evaluated to define the most suitable surface temperature and, thus, to select the PCM considering its phase change temperature.

Table 4. Radiant cooling panel's configurations (Adapted from [3])

None (N)	Back (B)	Side (S)	Side-Back (SB)	Side-Back-Side (SBS)
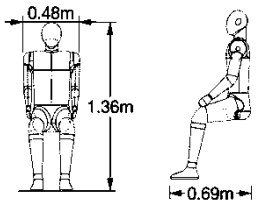	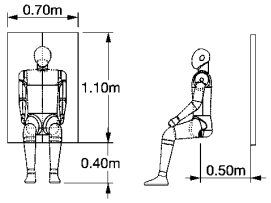	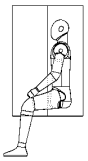	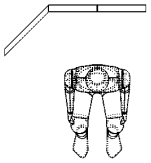	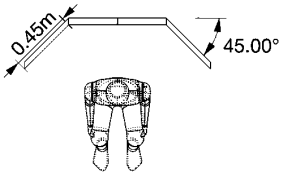

In parallel, a parameter tree and a full factorial experiment are defined to identify the contexts where it is feasible to implement the proposed radiant cooling strategy. The contexts are characterised by the climate represented by a location, i.e., Zurich (ZH) or Lugano, Ticino (TI); the type of office, i.e., an open-floor office layout; the size of the office, i.e., medium or large; the occupancy level and patterns, i.e., low, medium, or high; the envelope quality defined by the construction age, i.e., 1948, 1978, 1994, 2001, 2020; and the ventilation and cooling strategy, i.e., ventilation without cooling system available. Additional parameters such as appliances and lighting use are fixed according to SIA standards. The evaluation of the contexts is achieved using building performance simulations (see Section 4) and the following criteria:

i. During occupancy, the context has no more than 30% of hours with an indoor temperature over 26°C.

ii. When the outdoor temperature is higher than 26°C, the median indoor temperature is lower than 30°C.

iii. Due to high indoor temperatures, the percentage of dissatisfied people is lower than 40%.

In other words, this exploratory study identifies the scenarios where cooling is required to maintain thermal comfort, and there is a feasible number of people dissatisfied with the thermal environment who can use the mobile radiant cooling panel solution to restore comfort. In contexts where most people are uncomfortable, another cooling strategy must be implemented, e.g., fixed radiant cooling panels addressing the whole working space.

Finally, the results from the thermal comfort study and the exploratory cooling demand study are combined to estimate the energy-saving potential of the proposed radiant cooling system (see Section 5).

Figure 6 summarises the design and application space explored. On the top left are presented the two stages of the comfort study, and on the top right, the exploratory cooling demand study. These studies result in design decisions and application contexts, which are used to estimate the energy performance and energy-saving potential of the proposed occupant-centric mobile radiant cooling strategy. Additional and detailed information on the methods, models, simplifications and assumptions used to perform the study is presented in Section 3, i.e., comfort analysis, Section 4, i.e., energy performance analysis, and Section 5, i.e., feasibility study.

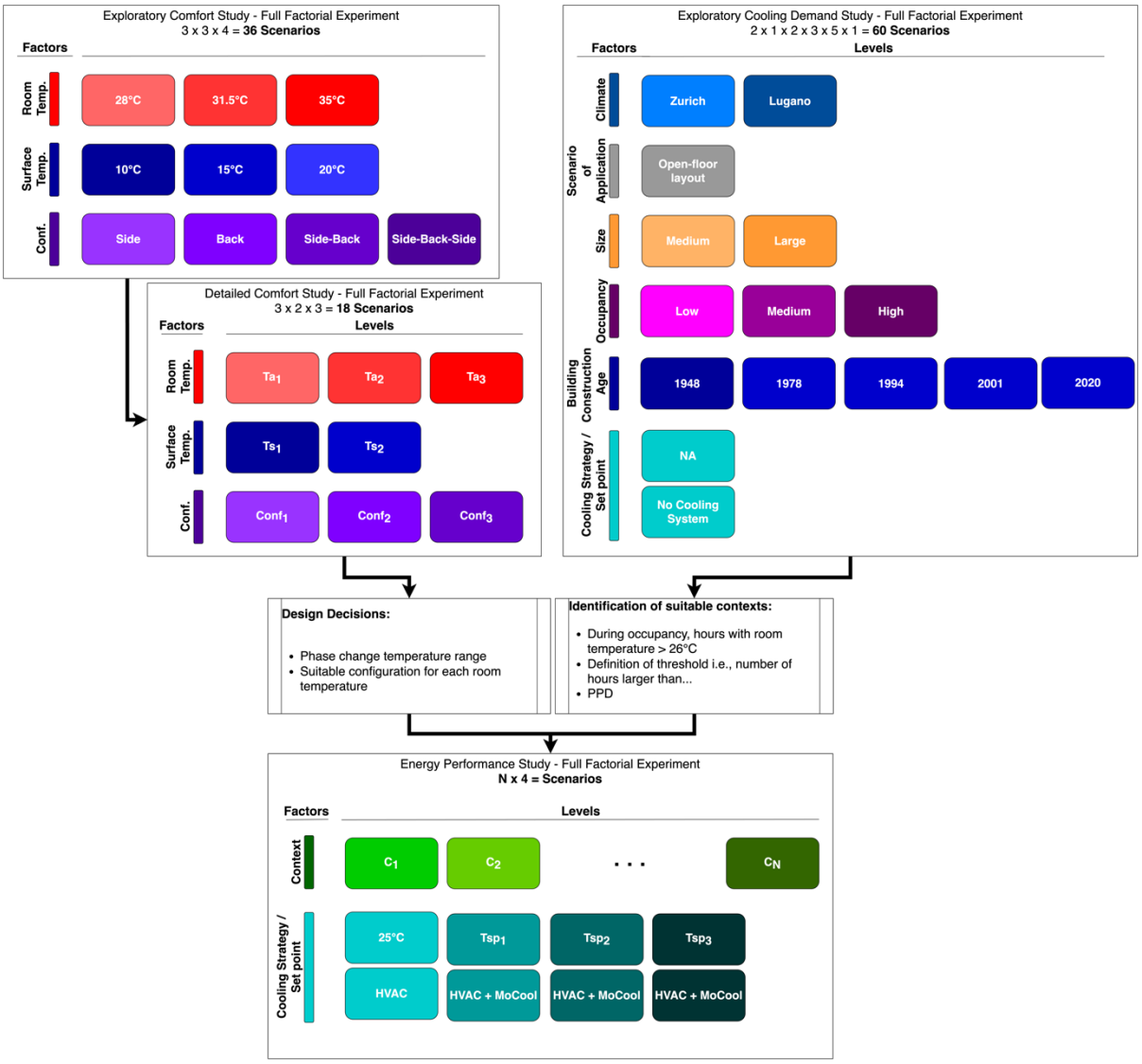

Figure 6. Design of Experiments

3 Comfort Analysis

The simulation-aided design process of the decentralised, occupant-centric radiant cooling panel is assisted by two different simulation strategies dedicated to each aspect of the performance analysis, i.e., thermal comfort and energy performance. As shown in Figure 6 (see Section 2.4), both analyses are performed in a two-stage process consisting of an exploratory and a detailed study; thus, the complexity level of the modelling strategies is adapted accordingly. This chapter describes the theory, numerical models, modelling assumptions and results of the design process concerning the comfort analysis of the PRCS. Furthermore, the methods, metrics, and case studies used in this chapter advance the state-of-the-art and have been peer-reviewed and published under the title “Integrating CFD and thermoregulation models: A novel framework for thermal comfort analysis of non-uniform indoor environments” in the scientific journal Energy and Buildings (see [3]).

3.1 Human thermoregulation

As described in [22], humans must maintain the core body temperature relatively constant, usually between 36.1°C and 37.8°C, for all the cellular functions to work correctly. Heat is transferred via the circulatory system between the core compartment, which contains all the organs more susceptible to temperature damage, and the peripheral shell, which consists of the skin and subcutaneous fat, to regulate the core body temperature. The thermoregulatory system triggers multiple mechanisms to promote heat loss, conservation, and generation. Ultimately, a balance must be reached between the metabolic heat production and the heat exchange between the body and the environment.

Considering a naked human at an ambient temperature of 21°C – 25°C, heat exchange with the surroundings is split into ~60% due to radiation, 20% by evaporation, 15% by convection, and 5% by conduction. Under a cold stimulus, peripheral vasoconstriction is triggered to reduce the amount of blood flowing through the peripheral shell to reduce the skin temperature. Consequently, the radiant, convective and conductive heat losses are reduced. Below a certain temperature threshold, additional heat generation is required to maintain the body's heat balance, for example, by modulating heat production or promoting muscle activity such as shivering.

Under a warm stimulus, peripheral vasodilatation increases the skin’s temperature, thus increasing radiant, convective, and conductive heat losses if the ambient temperature is lower than the body's. Above a certain temperature threshold, evaporative heat losses are increased via sweating. Considering these phenomena and thermoregulation mechanisms, a thermoneutral region is defined for ambient temperatures in which vasomotor responses control the core temperature, i.e., heat balance is reached solely by sensible heat transfer mechanisms. The temperature boundaries of this region depend on many factors, such as gender, age, clothing level, and ambient conditions. Nevertheless, as discussed in [23] and [24], providing conditions within the boundaries of the thermoneutral region is not enough to ensure thermal comfort, i.e., the span of environmental conditions that comprise the comfort region is smaller than the thermoneutral region.

The human thermoregulatory system can be modelled using mathematical formulations. The main models presented in the literature are briefly summarised in this section, based on the detailed work by Shine and Chithramol [25]. Starting in 1934, Burton [26] established a modelling basis where a cylindrical shape represents the human body, and the Fourier heat conduction equation describes the heat transfer. From there, advances were proposed to increase the number of segments, e.g., 2 in [27], establish the fundamental governing equation for heat transfer in living tissues [28], and include multiple segments and layers in [29].

Only after [30] the thermal regulation mechanisms were included in the mathematical models, followed by Stolwijk [31], where the thermoregulatory system is solved using control theory with negative feedback using a multi-segment (i.e., six body segments) and multi-node (i.e., four radial layers) representation of the human body. This model became an important milestone and the basis of subsequent models. For example, [32] increased the number of segments and layers to 15, [33] incorporated thermoregulation mechanisms as a function of mean skin and head core temperature, [34] and [35] integrated shivering models. More recently, [36] presented a comprehensive model integrating sweating distribution, fat tissue activity, ageing, and radiation. While previous models reproduce the one-dimensional nature of the heat flow, additional efforts have been made to capture the two- and three-dimensional nature. The reader is directed to [25] for a comprehensive description of the history and characteristics of thermoregulatory models.

3.2 CFD Model

The CFD model is implemented in OpenFOAM® v23.12 [37] to solve the indoor airflow and heat transfer. The geometric model of internal objects, e.g., manikin, radiant systems, furniture, and appliances, can be developed using external CAD tools and exported in stereolithography (STL) format. The discretisation of the computational domain, or mesh, can be developed using a combination of native

OpenFOAM® tools, i.e., BlockMesh and SnappyHexMesh [38]. Accordingly, from triangulated geometries, it is possible to create hexahedra-dominant meshes with high control of size distribution.

OpenFOAM® steady-state buoyant turbulent flow of compressible fluids solver, buoyantSimpleFoam, is chosen, which is coupled to the $k-\epsilon$ turbulence model, i.e., coupling the solution of the turbulent kinetic energy k and dissipation rate ϵ transport equations. Alternatively, if a transient problem is studied, the CFD model can be adapted to use the transient version buoyantPimpleFoam. The radiation heat transfer is solved using the Finite Volume Discrete Ordinates Method (fvDOM), which solves the radiative transfer equation for a finite number of discrete angles. A detailed description of these solvers can be found in [37].

A detailed description of these solvers can be found in [37]. Briefly, the mass conservation is implemented as in Equation 1, where u is the velocity field and ρ is the density field.

$$\nabla \cdot (\rho \mathrm{u}) = 0 \tag{1}$$

The momentum conservation is implemented as in Equation 2, where p is the static pressure field and g is the gravitational acceleration, μ_{eff} is the effective viscosity, and $D(u)$ is the deformation tensor defined as in Equation 3.

$$\nabla \cdot (\rho u u) = -\nabla p + \rho g + \nabla \cdot \left(2\mu_{eff} D(u)\right) - \nabla \left(\frac{2}{3}\mu_{eff}(\nabla \cdot u)\right) \tag{2}$$

$$D(u) = \frac{1}{2}(\nabla u + (\nabla u)^T) \tag{3}$$

The energy conservation is solved for the specific enthalpy h as in Equation 4. Here, K is the specific kinetic energy and α_{eff} is thermal diffusivity.

$$\nabla \cdot (\rho u h) + \nabla \cdot (\rho u K) = \nabla \cdot \left(\alpha_{eff} \nabla h\right) + \rho u \cdot g \tag{4}$$

Different boundary conditions can be defined, e.g., inlet air flows defined by their velocity and temperature, air outlet flows defined by the pressure, and heat transfer surfaces such as walls, lighting systems, electric appliances and radiant systems defined as adiabatic, with a fixed temperature, or with a fixed heat transfer rate. Radiant surfaces can be defined by their emissivity and the Marshak radiation condition to estimate the incident radiation field G. The manikin surface temperature is calculated within a Python program using a thermoregulation model to estimate the skin temperature and thermal resistances to account for the clothing insulation.

Finally, information must be stored and transferred from the CFD model to enable the coupling with the thermoregulation model, for example, the radiant and total heat flux integrated over the surface of each body segment and the average air velocity and temperature around the body segments. To this end, runtime function objects are defined.

3.3 Thermoregulation model

The joint system thermoregulation model (JOS-3) v0.5.0 [36] is integrated into the framework to calculate the human physiological responses to the indoor environment and radiant systems. JOS-3 is a detailed and opensource model implemented in Python that accounts for the age, gender, weight, and height in the calculation of the metabolic rate; it includes heat gain in the skin due to radiation; the heat transfer is calculated considering 85 nodes, i.e., central blood node, 17 artery nodes, 17 vein nodes, 12 superficial vein nodes, 17 core node, two muscle nodes, two fat nodes, and 17 skin nodes; it divides the human body into 17 segments, i.e., head, neck, pelvis, chest, back, and left and right shoulders, arms, hands, thighs, legs and feet; the heat production includes basal metabolic rate and external work, shivering and non-shivering thermogenesis; evaporative heat loss by sweating is included. Equation 5 presents the generalised heat balance equation for each node [3].

$$Cap_{j(i)}\frac{d}{dt}\left(T_{j(i)}\right) = Q_{j(i)} + B_{j(i)} - D_{j-j'(i)} - C_{j(i)} - R_{j(i)} - E_{j(i)} - RES_{j(i)} \quad (5)$$

Where Cap is the heat capacity, T is the temperature, t is the time, Q is the heat production, B is the heat exchange by blood flow, D is the heat exchange by conduction, C is the convective heat exchange, R is the heat exchange by radiation, E is the heat exchange by evaporation, RES is the respiration heat exchange. The subscript i represents the segment number, j represents the tissues and j' the adjacent body tissue.

The model inputs are the personal characteristics, i.e., height, weight, fat percentage, age, sex, cardiac index, and the environmental parameters, i.e., ambient temperature, mean radiant temperature, air velocity, relative humidity, clothing insulation, physical activity ratio, and posture. The environmental parameters can be defined for the whole body or vary across the 17 body segments, allowing for the assessment of non-uniform environments. Finally, the model outputs more than 50 parameters, including total heat production of the whole body, heat loss by respiration and from the skin of the body part, i.e., total, sensible and latent heat losses, core and skin temperature of the body part, mean skin temperature of the whole body, local and mean skin wettedness (for a detailed model description, refer to [36]).

3.4 Coupling Scheme

The open-source coupling library preCICE v3.1.1 [39] and the OpenFOAM adapter [40] combine the CFD model implemented in OpenFOAM with the human thermoregulation model JOS-3 implemented in Python. preCICE enables the creation of partitioned simulations using an efficient and scalable black-box coupling of different participants, i.e., independent models. Figure 7 shows the coupling scheme designed. The CFD simulation is defined by one fluid participant using the conjugate heat transfer (CHT) module and 17 interfaces, i.e., the 17 body segments with their corresponding meshes. Accordingly, 17 solid participants were defined using a Python program. In this case, only one mesh is generated and owned by the fluid participant; the mesh of each body segment is sent to each solid participant.

The fluid participant is configured to read the temperature and write the heat flux fields of all interfaces. Conversely, the solid participants write the temperature and read the heat flux field. A parallel explicit coupling scheme is set using 17 communication sockets where the first participant is the fluid participant and the second is one of the solid participants, enabling an efficient parallel solution of the whole co-simulation.

Using function objects executed at each iteration within OpenFOAM, the total and radiant heat fluxes are integrated across the interface for each body part, and the average air temperature and velocity values are calculated. The Python program retrieves the information of all the body segments and generates the MRT (MRT), air temperature (T_a) and air velocity (V_a) vectors, required as inputs in the thermoregulation model.

$$MRT = \begin{bmatrix} MRT_{head} \\ \cdots \\ MRT_{l\_foot} \end{bmatrix}; T_a = \begin{bmatrix} T_{a\_head} \\ \cdots \\ T_{a\_l\_foot} \end{bmatrix}; V_a = \begin{bmatrix} V_{a\_head} \\ \cdots \\ V_{a\_l\_foot} \end{bmatrix}$$

The MRT of each body segment is estimated using the radiant heat transfer of each body segment using Equation 6 [41].

$$MRT_i = \left(\left(\frac{Q_{rad_i}}{e_i * \sigma * A_i}\right) + T_i^4\right)^{0.25} \quad (6)$$

Where, T_i is the surface temperature of the body segment at the previous iteration, σ is the Stefan-Boltzmann constant, e_i is the emissivity of the body part, Q_{rad_i} the radiation heat flux integrated over the body segment, and A_i is the surface area of the body segment. After, the new environment is defined, i.e., MRT, T_a and V_a, it is updated and simulated in JOS-3 to estimate the new thermoregulatory

state. Each solid participant retrieves the skin temperature of the corresponding body part, calculates the new surface temperature, i.e., using the thermal resistance of the clothing, and transfers the value to the CFD boundary condition. The coupling continues until a convergence criterion, e.g., skin temperature variation below a threshold or the maximum number of iterations, is reached.

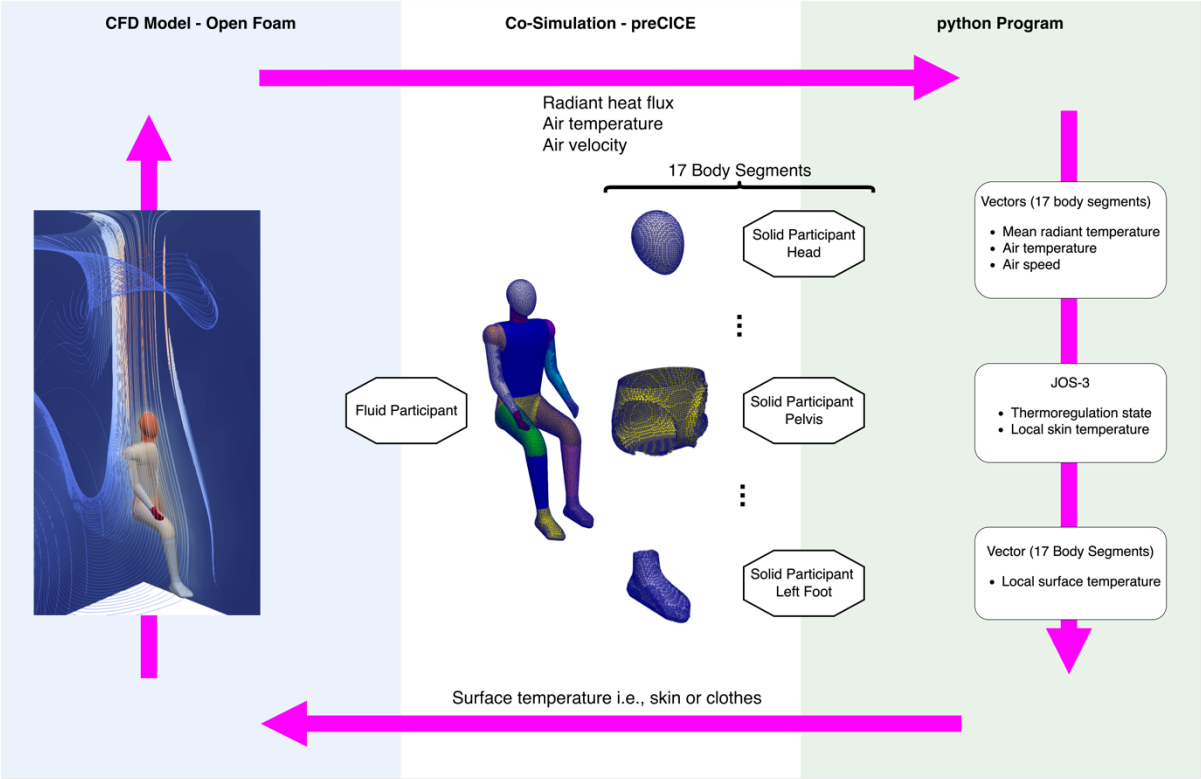

Figure 7. Coupling scheme: Co-simulation of CFD and thermoregulation model (Figure taken from [3]).

This framework is designed to be flexible, adaptable and scalable. Accordingly, different modules, models, and data transferred could be added or removed depending on the complexity and accuracy required. For example, mass transport and exchange models could be added to account for the latent load in the CFD and thermoregulation models so that the interaction and impact of air relative humidity, sweating, respiration, and condensation could be estimated in detail.

3.5 Comfort Metrics

The PMV index, based on Fanger's human heat balance equation [42], has been globally applied across all building types to evaluate thermal comfort despite its application being intended for HVAC design [43]. Further, it is aimed at the uniform and steady-state indoor environment and does not consider the effect of local cold or hot sensation on the overall thermal sensation [42]. As observed in [6], [7], the validity of the PMV needs to be thoroughly assessed under these conditions. Consequently, alternative comfort metrics are required to evaluate thermal comfort in non-uniform indoor environments, such as the one produced by PRCS. To this end, the following metrics are selected and defined to understand the impact of radiant cooling on human thermal comfort. These are based on empirical and statistical comfort studies:

i. **Local and mean skin temperatures** are crucial elements in the study of thermal comfort, as they directly reflect the heat exchange process of the human body [44]. Several studies have found direct relationships between mean skin temperature and overall thermal sensation [45].

ii. ***Local and mean skin wettedness*** are measures of the proportion of the skin that is wet at each body part and, on average, for the whole body. An upper limit of 0.3 has been established, below which thermal comfort can occur [46].

iii. ***Radiant temperature asymmetry*** is defined in the literature as the difference between the plane radiant temperature of the opposite sides of a small plane element describing the asymmetry of the radiant environment [47]. This metric directly correlates with the percentage of dissatisfied people [48]. In the case of cool walls and accepting that 5% of the people are feeling uncomfortable, a limit for the temperature asymmetry of 10 K has been found. In this study, exploiting the resolution and discretisation of the human body in the CFD and thermoregulation model, two radiant asymmetries are defined considering the MRT directly estimated over the different body parts. In this case, a frontal radiant asymmetry $\Delta T_{r-frontal}$ is estimated as the difference between the MRT of the chest and the back of the manikin, and a lateral radiant asymmetry $\Delta T_{r-lateral}$ is estimated as the maximum difference between the MRT of the right and left parts of the body (i.e., shoulder, arm, hand, tight, leg, foot).

Further, based on the human heat balance and the thermal equilibrium of the human body with the indoor environment, the following human-centric physic-based comfort metrics are defined:

iv. ***Reference heat deviation (RHD)*** is a metric proposed in this study to quantify the differences in the human heat balance due to changes in the indoor environment. As described in Section 3.1, to maintain the heat balance, the thermoregulation system activates mechanisms to modulate the heat produced by the body and dissipate it to the environment. Jos-3 models the total heat produced by the human body including:

- The basal metabolic heat: the heat necessary for vital functions and systems to work.
- The heat produced by work.
- The heat produced by shivering thermogenesis: coordinated and involuntary rhythmic muscle contractions.
- The heat produced by non-shivering thermogenesis: activation of brown adipose tissue (BAT).

Personal characteristics and activity levels define the basal metabolic heat and the heat produced by work. Shivering and non-shivering thermogenesis are part of the thermoregulatory mechanisms; the warmer the environment, the lower the heat production by shivering and non-shivering thermogenesis. Further, the skin temperature is modulated to increase sensible heat dissipation by conduction, radiation, and convection. After that, latent heat dissipation needs to be enhanced, for example, by sweating and increasing evaporative heat transfer. Thermal comfort can be achieved when the temperature can be regulated to enhance sensible heat transfer. A reference metabolic heat production and sensible heat losses are defined under indoor conditions that ensure thermal neutrality without using the PRCS. The deviation from these values is then calculated under new environmental conditions and the presence of PRCS. Ultimately, the **RHD** is defined as the sum of two metrics: the **metabolic heat deviation (MHD)** and the **sensible heat deviation (SHD)** from the reference condition.

v. ***Reference heat deviation temperature (RHDT)*** is a metric proposed in this study to translate the information captured by the RHD metric into temperatures that enable an understanding of the impact of radiant systems at building and building system levels. For example, in the case of studying the impact of the PRCS in combination with an HVAC system, the RHDT represents the temperature to which the HVAC needs to condition a specific space to produce the same impact on the human heat balance as the PRCS. To calculate the RHDT, the relationship between the RHD and the indoor environmental conditions is investigated in scenarios where no PRCS is used. The relevance of this metric lies in that it captures the effect of the radiant systems in combination with specific ventilation strategies, e.g., natural ventilation, HVAC system, in specific indoor environments, e.g., characterised by specific radiation distribution from windows and walls.

3.6 Case study description

A virtual single office room is simulated under different air temperatures, combined with a vertical PRCS. The room is assumed to have no windows, a floor area of 25m^2 and a height of 3m, and it is ventilated using a controlled inlet airflow and a pressure outlet flow located in the ceiling. The supply air enters at low momentum, so the ventilation generates no draught. Further, the office room is assumed to be in thermal equilibrium with adjacent spaces at ambient air temperature. One occupant is sitting in the centre of the room performing office work. Different PRCS are tested by varying their surface temperature, surface area, view factor, and room air temperature. The air velocity, relative humidity, and personal characteristics of the occupant remain constant across the experiments. Table 4 (see Section 2.4) presents the five PRCS configurations tested with their placement relative to the occupant: (N) represents the baseline without any PRCS; (B) with one vertical panel with an effective area of 0.77m2, located 0.5m at the back of the occupant, and 0.4m above the ground; (S) with the vertical panel located 0.5m at one side of the occupant; (SB) that adds a wing of 0.45m to one side of the (B) configuration with 45°, resulting in a total radiant area of ≈ 1.3m2; (SBS) that adds a second wing to the opposite side for a total radiant area of ≈ 1.8m2.

The computational domain is developed using a manikin adapted from [49] (see Table 4 – N, Section 2.4), and the mesh is generated using blockMesh and snapyHexMesh [38]. Figure 8 (left) shows an example with the PRCS configuration SBS, where the colours identify the boundary conditions. Figure 8 (right) shows the resulting highly structured hexahedra-dominant mesh with perpendicular layers inflated from the manikin and PRCS surfaces to enhance the thermal and fluid flow boundary layer's solution. Further, a grid independence study is performed to find the mesh parameters that balance the computational cost and accuracy. This results in corresponding 1.1M, 1.5M, 1.5M, 1.7M, and 2M elements for the configurations N, B, S, SB, and SBS.

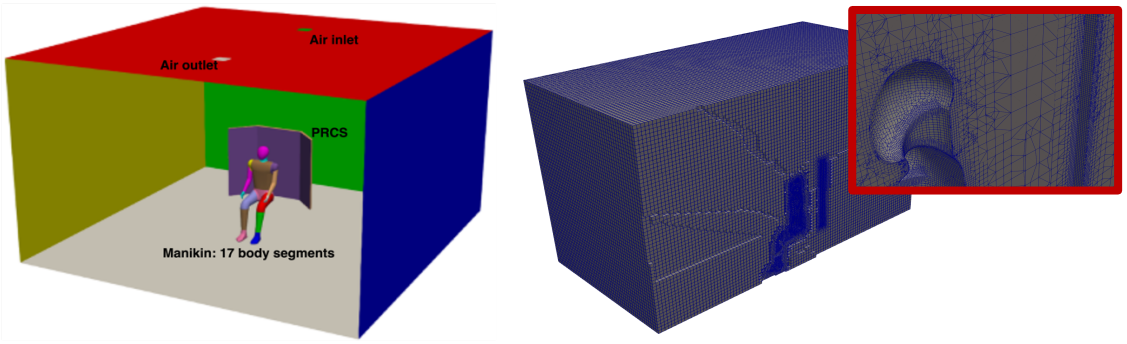

Figure 8. Computational domain (Left) – Mesh (Right) (Figure taken from [3])

Table 5 summarises the velocity and temperature boundary conditions set, along with the emissivity values. The emissivity values for the naked body parts, i.e., head, neck and hands, are 0.98, and the clothes are 0.75, taken from [50] and [51], respectively. Further, the CFD simulation is initialised using the air inlet values, which correspond to a constant air velocity of 0.2m/s and an air temperature T_{air}. For the manikin temperature, the initial temperature corresponds to the skin temperature calculated using the thermoregulation model for a uniform operative temperature, MRT equal to the tested air temperature and a relative humidity of 50%.

Regarding the thermoregulation model, the manikin represents a 30-year-old male with a weight of 60kg and a height of 1.7m. A sitting position is assumed for performing office activities corresponding to 1.1MET. The clothing thermal resistance is set to 0clo for the naked parts and 0.5clo for the rest, assuming typical values of summer clothing (thermal resistance of $1clo = 0.155\, m^2K/W$).

Table 5. Boundary Conditions (Adapted from [3])

Object	Velocity	Temperature	Emissivity
Walls (4x)	No slip	Uniform: T_{air}	0.9
Ceiling	No slip	Uniform: T_{air}	0.9
Floor	No slip	Adiabatic	0.9
Inlet	Uniform: 0.2m/s	Uniform: T_{air}	-
Outlet	Outflow	Outflow	-
PRCS	No slip	T_s	1
Manikin – Each body segment	No slip	JOS3	0.98: Naked body; 0.75: Clothing

3.6.1 Baseline simulation

A baseline simulation is performed by reproducing an environment where thermal comfort is achieved using only the ventilation system. While literature shows that comfort temperature ranges vary depending on conditions such as the type of activity, outdoor temperature, personal characteristics and preferences [52], an inlet air temperature of 25°C, velocity of 0.2m/s and relative humidity of 50% is set.

Figure 9 shows each body segment's calculated mean skin and cloth temperatures. While the thermoregulation model calculates the skin temperature given the environmental parameters, the clothes' temperature is calculated by the Python program and updated in the CFD boundary conditions. Additionally, there is a radiant heat exchange between the body segments because they have different temperatures. This phenomenon is particularly noticeable around the neck, between the arms and lateral sides of the chest and back, and over the thighs, and impossible to capture if a mean skin temperature is imposed over the whole body, as is usually done in CFD simulations and experiments with thermal manikins. The radiant heat flux density is negative, indicating heat loss from the body to the ambient, which naturally is higher in the naked body parts, i.e., hands, head and neck.

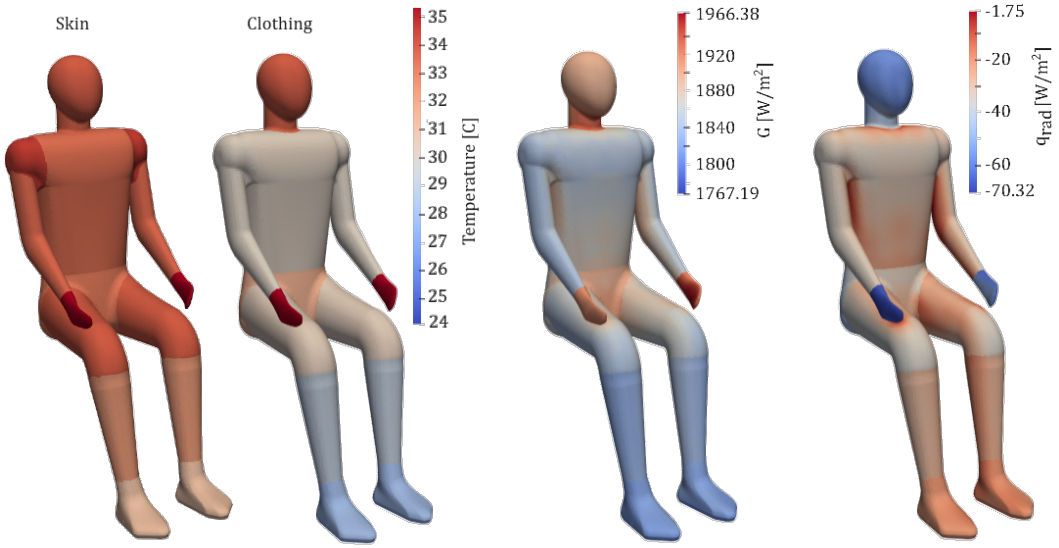

Figure 9. Baseline case: Temperature and radiation fields

Considering that the manikin has a total surface area of 1.53m^{2,} and assuming a metabolic rate of 1.1MET (sitting, office activity), the subject would produce around 63.8W/m^2 [61], i.e., 97.61W, and in this case, the thermoregulation model estimates 64.5W/m^2, i.e., 98.72W. Further, the total sensible heat loss from the manikin to the environment estimated by the thermoregulation and by the CFD-model is, in both cases 76.5W. Consequently, the simplification of average values for the velocity and temperature fields and default heat transfer coefficients used in the thermoregulation model are supported. Further, the PMV and PPD are calculated, resulting in -0.13 and 5.4, respectively, indicating a comfortable environment.

Additionally, with the proposed framework, it is possible to estimate the thermoregulatory state of the subject in detail, with parameters calculated at local and whole-body levels. Table 6 summarises the key metrics. In this case, the body's metabolic heat is dissipated with 8.67% by respiration, 13.83% by latent and 77.50% by sensible losses through the skin. The radiation heat losses correspond to 61.1% of the sensible heat losses. Further, the body's mean skin temperature and wettedness are within the thermal comfort ranges.

Table 6. Thermoregulatory state at @25°C (Adapted from [3])

Metric			Value
	Metabolic heat	Q_M [W]	98.72
	Respiration heat loss	Q_R [W]	8.56
	Total skin heat loss	Q_{sk-T} [W]	90.16
	Latent skin heat loss	Q_L [W]	13.65
	Sensible skin heat loss	Q_S [W]	76.51
	Radiant skin heat loss	Q_{Rad} [W]	47.50
	Mean skin temperature	$T_{sk-mean}$ [°C]	33.61
	Mean skin wettedness	$W_{sk-mean}$ [-]	0.06

3.6.2 Exploratory comfort analysis

As described in Section 2.4, an exploratory design is established to understand the impact of main parameters on thermal comfort performance. Specifically, 36 cases result from the combination of the parameters presented in Figure 10.

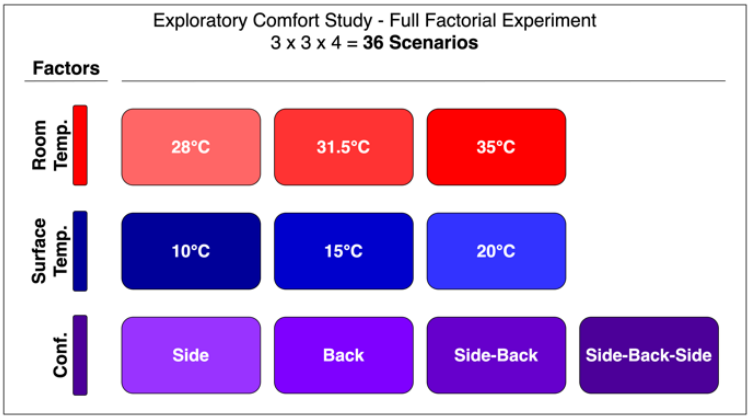

Figure 10. Exploratory comfort analysis – Design parameters

The first parameter is the room temperature, which ranges from 28 to 35°C to reproduce conditions that can be translated into different cooling setpoints and climate regions. The second parameter is the surface temperature of the active part of the radiant panel. This is related to the melting temperature of the PCM inside the radiant panels and its different layers. Finally, the radiant panel configuration is studied to understand what area and view factor are required and how the panel's performance changes with its relative position to the occupant. To this end, an emissivity of 0.8 is assumed for the radiant cooling panels, which can be achieved by painting its surface to increase the performance of, for example, an aluminium sheet [53]. Additional parameters and boundary conditions are set as in the baseline simulation (see Section 3.6).

Three additional simulations are conducted to assess the resulting heat balance when increasing the air temperature and excluding the radiant panels. It is important to underscore that in this exploratory study, the modelling complexity of the numerical framework is reduced by fixing the boundary

condition at the surface of the manikin with the temperature calculated through the thermoregulation model for the baseline simulation. In other words, communication between the thermoregulation and CFD models is established as unidirectional, which oversimplifies the active and passive measures that the body's thermoregulatory system employs to maintain its core temperature. Nevertheless, it clearly indicates the effect of the radiant cooling panel and, thus, serves the purpose of the exploratory study.

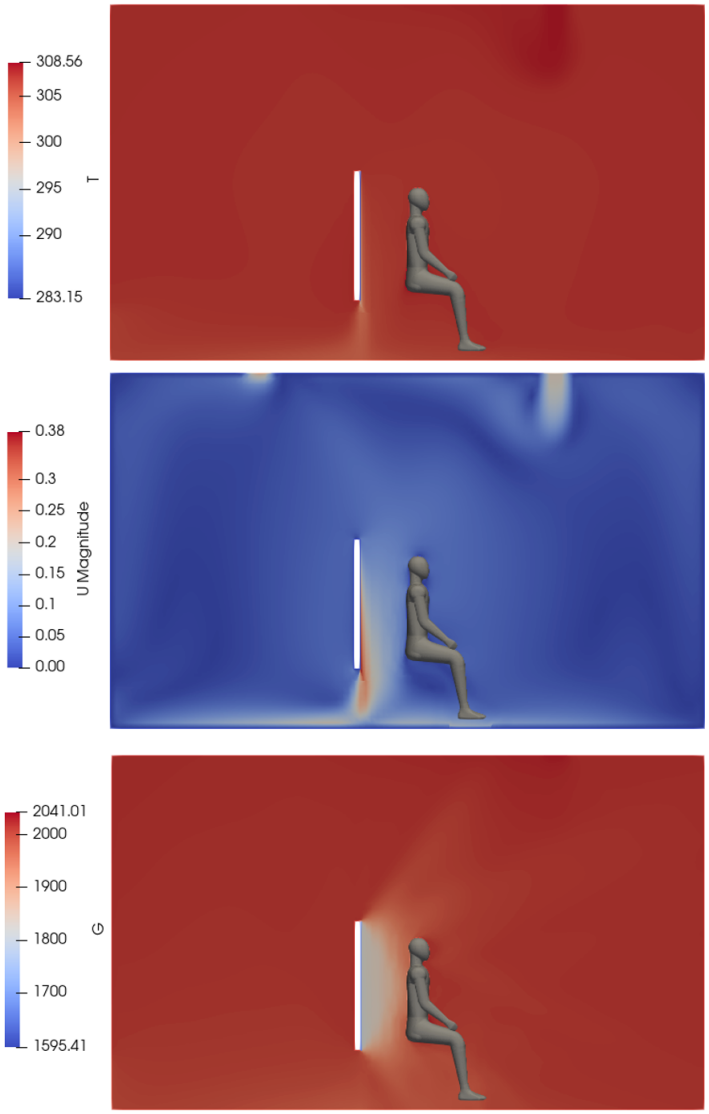

Figure 11. Indoor environment with a radiant cooling panel

First, for illustrative purposes, Figure 11, shows the results of the temperature (T [K]), velocity (U [m/s]), and the incident radiation (G [kg/s^3]) for one of the cases, i.e., the case with an ambient temperature of 35°C, one single flat radiant panel located in the back of the manikin, with a surface temperature of 10°C. While different cases have different magnitudes, the results are qualitatively similar for all the cases.

Figure 11 (top) shows the temperature and (middle) the velocity fields. The buoyant effect can be observed due to air temperature differences near the radiant panel. This is because the temperature of the air in contact with the panel decreases, causing an increase in density, and thus, it flows down. The air velocity observed near the panel has the same order of magnitude as the experiments reported in the literature [7]. It is also observed that this convective cooling has a minimum effect on the air temperature distribution and stratification. Consequently, the impact of the radiant cooling panel on

the manikin heat balance is mainly due to radiation. Figure 11 (bottom) shows the incident radiation field, where the influence of the radiant panel can be seen. All the surfaces facing the panel are expected to have an impact, with a more significant effect on the back, where the radiation is concentrated.

Figure 12 shows the incident radiant field on a horizontal cross-section located 0.6m over the floor to compare the influence of the different radiant panel configurations tested. Starting on the top-left corner and moving clockwise, Figure 12 shows the single panel located in the back (B), single panel located on one side (S), one-side extended panel located on the back (SB), two-side extended panel located in the back (SBS). Naturally, configurations B and S have a similar field of influence since they have the same panel with different orientations. Nevertheless, a different impact is expected, considering the exposed surface of the manikin in each case. With the panel extensions in SB and SBS, a higher concentration of radiation can be observed over the manikin and the panel.

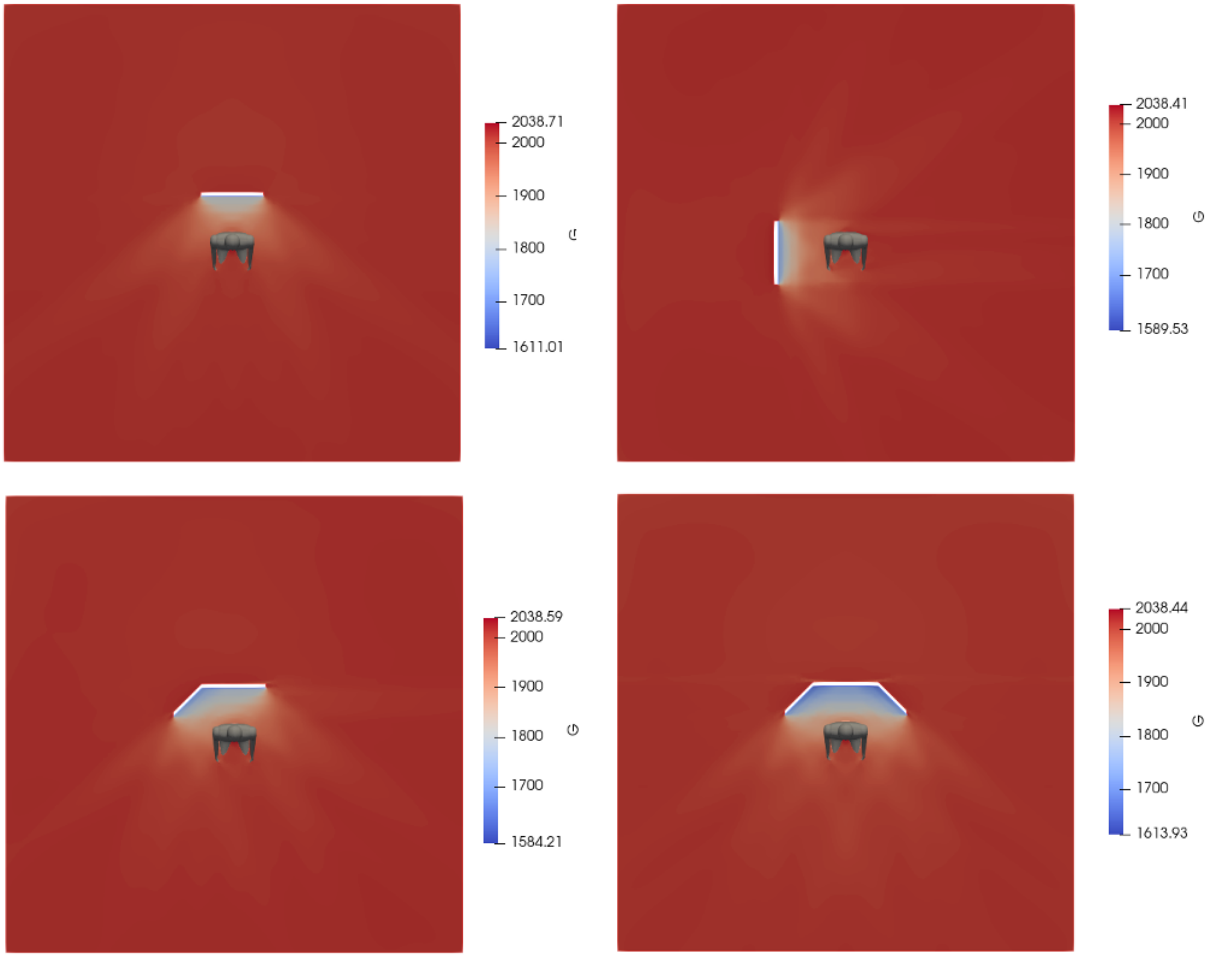

Figure 12. Radiant cooling panel field of influence

The qualitative effect of the radiant panels on the manikin can be observed in Figure 13, where the radiative heat flux (qr [W/m^2]) over the manikin's surface is shown. Each row corresponds to a different radiant cooling panel configuration (i.e., from top-down Configuration B, S, SB, SBS). In all the cases the ambient temperature is set to 35°C and the radiant panel surface temperature to 10°C. Negative values indicate heat losses and positive values indicate heat gains. Considering the heat losses (minimum values), configuration S has the smaller effect (-46.86 W/m^2), followed by Configuration B (-61.99 W/m^2), then Configuration SB (-81.05 W/m^2), and the greatest effect with Configuration SBS (-90.96 W/m^2). Further, it is observed that there is a low influence of the radiant panels over the legs and feet in all the configurations but Configuration S. When the panel is located on the side, it has

enough view factor to slightly influence the exposed leg. Moreover, the feet have the lowest temperature compared to the ambient, thus the highest heat gain.

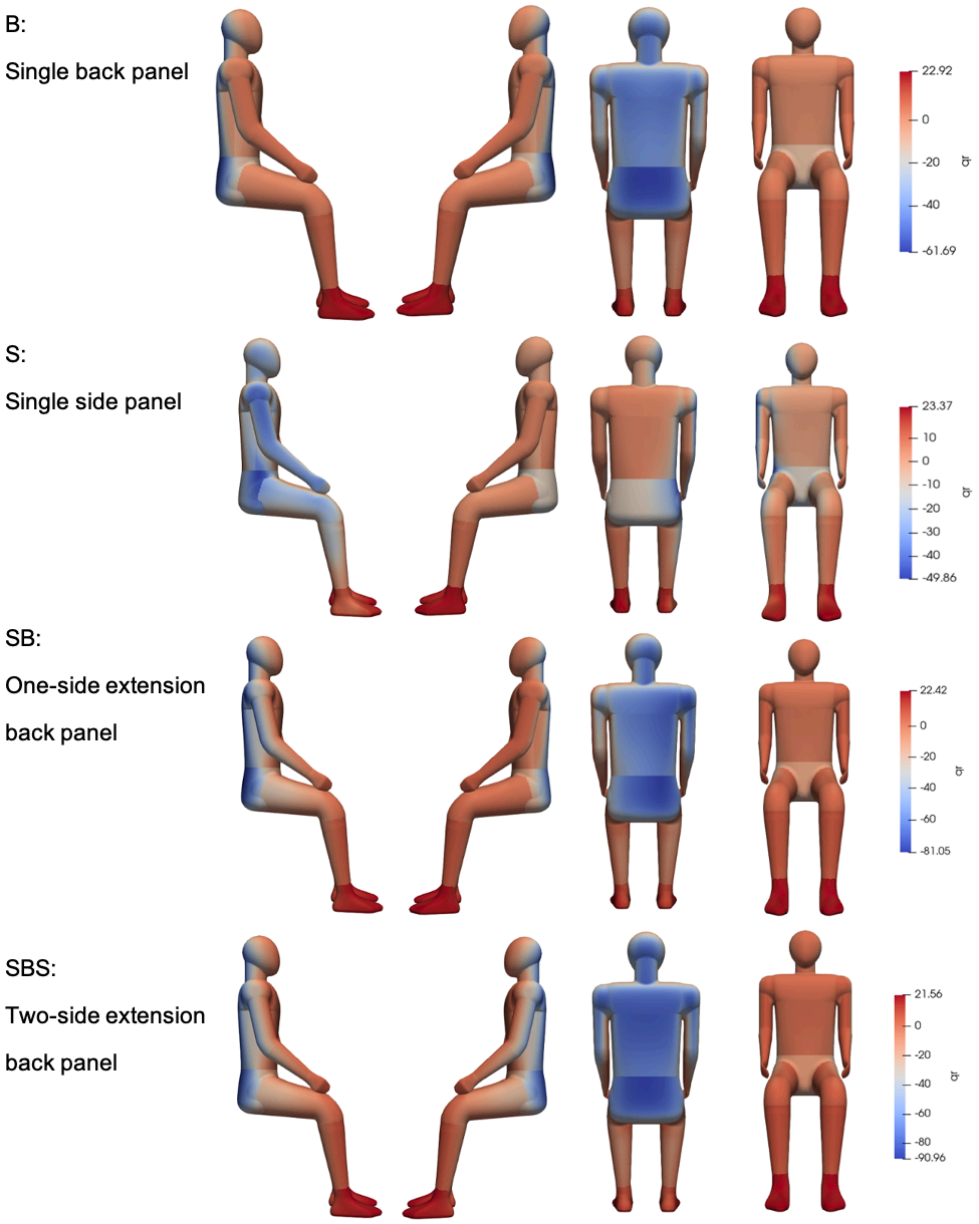

Figure 13. Manikin's radiant heat flux: Configuration B, S, SB, SBS (Top-Down); Ambient temp. 35°C, Radiant panel surface temp. 10°C.

Finally, a comparison of the performance of all the simulated cases is presented in Figure 14. Here, the heat balance of the manikin is calculated as the heat produced by a sitting human body with 1.2MET minus the heat dissipated across the surface. It is plotted against the total cooling power of the radiant panels. The dotted lines represent the heat balance for the reference simulations without the radiant panels when the room is at 28°C, 31.5°C and 35°C, and from there the second vertical axis is derived, representing the apparent air temperature given by the effect of the radiant panel. The type of marker represents the configuration tested i.e., B, S, SB, SBS. The size of the marker represents the active surface's temperature of the radiant panels.

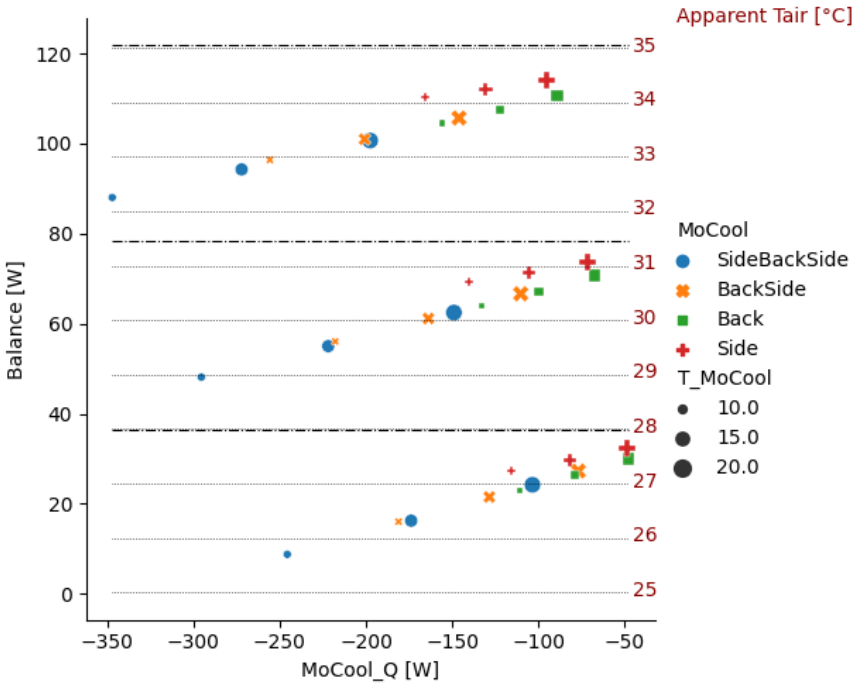

Figure 14. Radiant cooling panel performance

Interesting conclusions emerge from Figure 14. First, the radiant cooling panel's view factor, area, and location significantly influence the cooling effect. S has the least impact since the manikin has the smallest exposed area and view factor. It's closely followed by B, where a slight improvement arises from an increase in the manikin's exposed surface area. Considering these configurations, lowering the panel's temperature has a limited effect on its performance. At moderate ambient temperatures, the single back panel at 20°C has the same effect as the side panel at 15°C. However, as the ambient temperature rises, the single side panel requires a lower temperature to achieve equivalent performance. Additionally, these configurations reduce the apparent ambient temperature by approximately 1°C, aligning with findings from the literature (for example in[6].

The increase in effective area and view factor of SB and SBS significantly influences the panel's performance. With a panel temperature of 20°C, SB performs at least as well as S at the lowest temperature tested. Similarly, SBS with the highest surface temperature tested (i.e., 20°C) demonstrates equivalent performance to SB at 15°C surface temperature. Finally, the most significant effects of SB and SBS achieve a maximum reduction in apparent air temperature of around 2°C and 2.5°C, respectively. This means that at moderate air temperatures, specifically 28°C, SBS can lower the apparent air temperature to acceptable comfort ranges, i.e., below 26°C, with a cooling capacity of 250W.

3.6.3 Detailed analysis

The results of the explorative analysis presented and discussed in Section 3.9 are used to refine the design space. First, at high room temperatures, the tested PRCS configurations show only marginal improvement; that is, the radiant panel needs to be combined with other cooling strategies to ensure comfort. Second, the configuration S – one single panel located on the side of the occupant – has a limited impact due to the relatively small exposed area of the occupant. Third, when the panels are cooling at a high surface temperature of 20°C, their impact is minimal. Accordingly, the design space is refined as shown in Figure 15. While the relative humidity, air velocity and personal characteristics remain constant across the experiments, it is varied the PRCS surface temperature, i.e., 10 °C and 15°C, the ambient temperature, i.e., 26°C, 28°C, 30°C, and the PRCS configuration, i.e., B, SB, SBS. For each air temperature tested, a reference simulation without PRCS is included. Accordingly, 18 and 4 reference scenarios are evaluated (see Table 7).

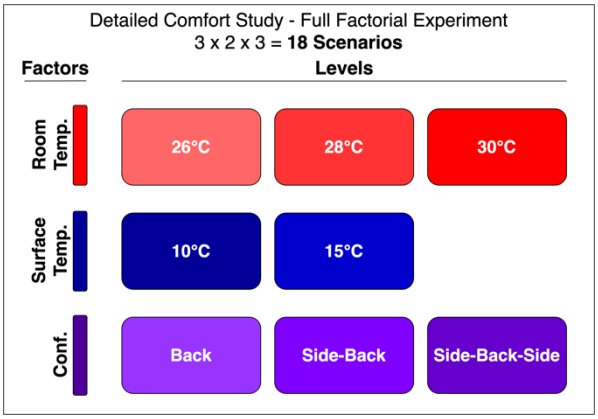

Figure 15. Detailed comfort analysis – Design parameters

Table 7. Detailed comfort analysis - Scenarios evaluated

Simulation ID	Tair [°C]	PRCS Configuration	PRCS Ts [°C]
C0_Ta25-N	25	N	NA
C1_Ta26-N	26	N	NA
C2_Ta26-B-Ts15	26	B	15
C3_Ta26-B-Ts10	26	B	10
C4_Ta26-SB-Ts15	26	SB	15
C5_Ta26-SB-Ts10	26	SB	10
C6_Ta26-SBS-Ts15	26	SBS	15
C7_Ta26-SBS-Ts10	26	SBS	10
C8_Ta28-N	28	N	NA
C9_Ta28-B-Ts15	28	B	15
C10_Ta28-B-Ts10	28	B	10
C11_Ta28-SB-Ts15	28	SB	15
C12_Ta28-SB-Ts10	28	SB	10
C13_Ta28-SBS-Ts15	28	SBS	15
C14_Ta28-SBS-Ts10	28	SBS	10
C15_Ta30-N	30	N	NA
C16_Ta30-B-Ts15	30	B	15
C17_Ta30-B-Ts10	30	B	10
C18_Ta30-SB-Ts15	30	SB	15
C19_Ta30-SB-Ts10	30	SB	10
C20_Ta30-SBS-Ts15	30	SBS	15
C21_Ta30-SBS-Ts10	30	SBS	10

To illustrate the impact of the PRCS on the indoor environment, Figure 16 presents the air temperature, air velocity, and incident irradiance fields for simulation C21. In this simulation, the inlet air temperature is 30°C, the PRCS surface temperature is 10°C, and the PRCS configuration is SBS. The temperature difference between the air and the PRCS induces a buoyant flow, which can be observed in the results. Despite this being the most extreme case simulated—featuring the highest air temperature and the lowest PRCS surface temperature—the highest air velocity is confined to a region within 5 cm of the PRCS, leaving the manikin unaffected. As a result, the risk of discomfort due to draught is negligible. This finding aligns with the results presented in [14]. Furthermore, the air temperature remains largely homogeneous at the defined inlet temperature, showing no significant stratification. Thus, the primary impact of the PRCS is attributed to radiative heat exchange. Finally, the radiation field's influence is observed to be localized, primarily affecting the occupant’s upper body.

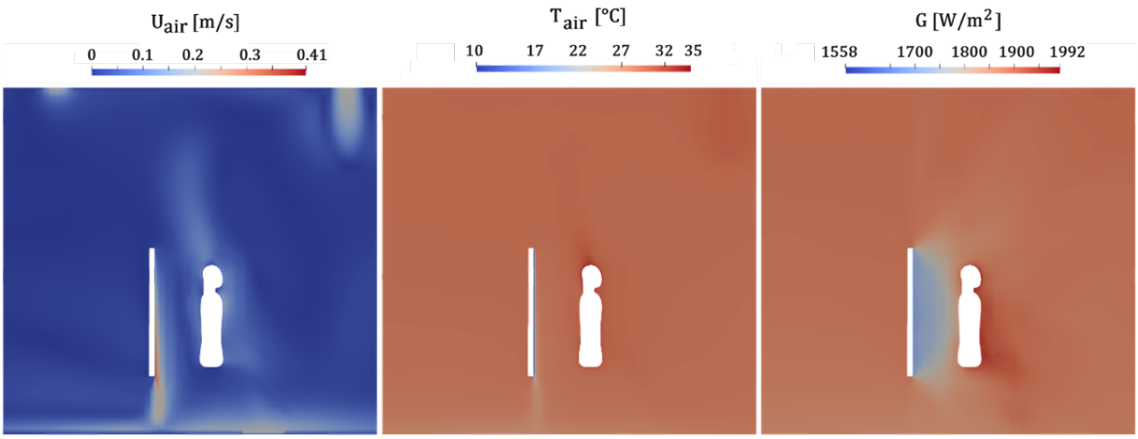

Figure 16. Impact of PRCS on the indoor environment in the simulation C21 (Tair: 30°C, PRCS: SBS, Ts: 10°C). Left: Velocity field (U); Middle: Air temperature (T_{air}); Right: Incident irradiance (G). (Figure taken from [3])

Figure 17 illustrates the radiant heat exchange over the manikin in simulation C19, an extreme scenario designed to assess the impact of radiant asymmetry. In this simulation, the inlet air temperature is set to 30°C, the PRCS surface temperature is 10°C, and the SB PRCS configuration generates radiant asymmetries in both the frontal and lateral planes of the manikin. Overall, the radiant heat exchange results in a maximum temperature difference of approximately 80 W/m² between the front and back of the manikin, primarily due to the PRCS panel positioned behind it. This effect is most pronounced on the posterior side of the head, neck, pelvis, shoulders, arms, and back. While the lower limbs—including the thighs, legs, and feet—are also affected, the impact is notably weaker compared to the upper body. Additionally, lateral asymmetry significantly influences the shoulders and arms, has a lesser effect on the thighs, and is negligible in the legs and feet.

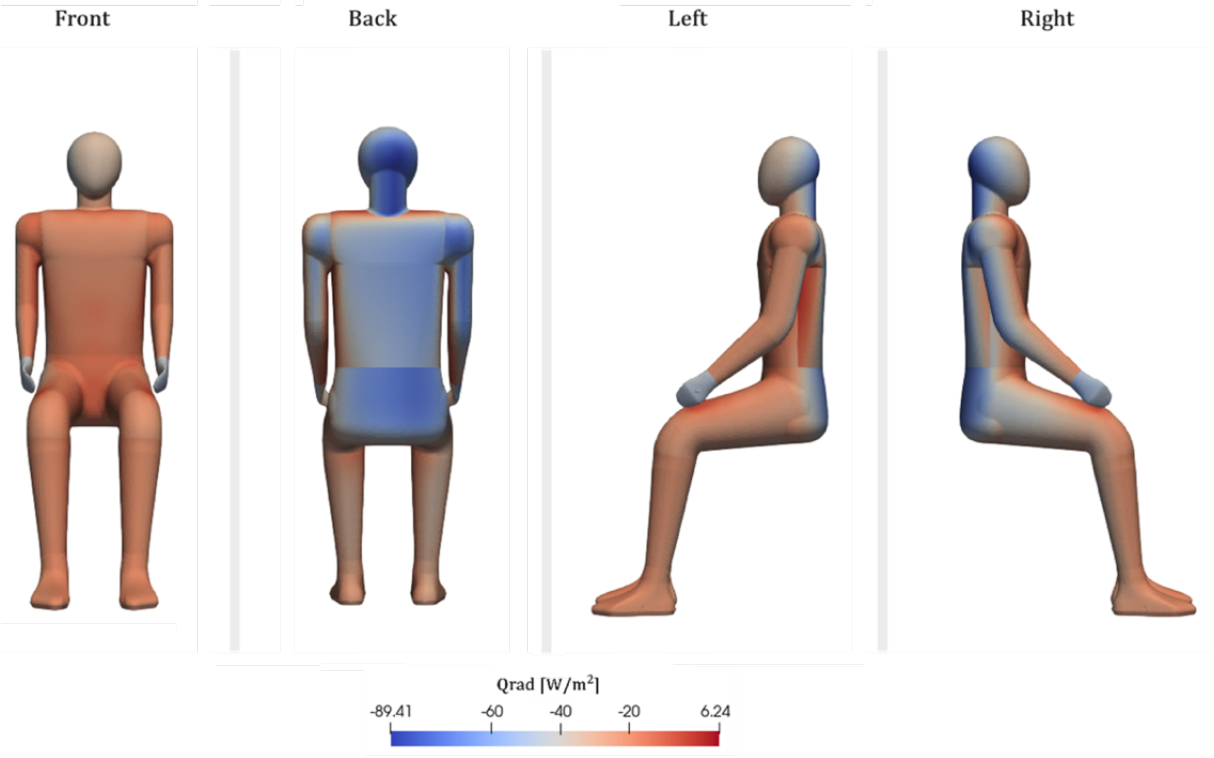

Figure 17. Radiation heat flux at the manikin's surface in the simulation C19 (Tair: 30°C, PRCS: SB, Ts: 10°C). (For optimal interpretation, refer to the colour version of this figure) (Figure taken from [3])

Human heat balance: RHD and RHDT

Figure 18 explores in detail the impact of the PRCS on human heat balance using the newly proposed RHD and RHDT metrics. As explained in Section 3.1, the human body's thermoregulation system has several mechanisms to maintain a virtually constant core body temperature. These mechanisms modulate the rate of heat produced by the body (Q_M), sensible heat losses (Q_s) through conduction, convection, and radiation, and latent heat losses (Q_l) through sweating and respiration (Q_R). On the left side of Figure 18, the amount of heat produced by the body and the proportion dissipated by each mechanism are shown. On the right side, the differences between the reference Q_{M_Ref} (at the baseline simulation) and the simulated Q_M, i.e., MHD, as well as the differences between the reference Q_{s_Ref} (at the baseline simulation) and the simulated Q_s, i.e., SHD, are displayed. Summing these two values results in the proposed RHD index.

At an air temperature of 26°C, the contribution of each dissipation mechanism remains approximately constant, with about 8.6% by respiration, 13.8% by latent losses, and 76.6% by sensible losses, yet a variation on Q_M is observed. From the baseline simulation, where 98.7W are produced, Q_M decreases by 3.8W to 94.9W at 26°C without PRCS. Using the PRCS, the change in Q_M varies from a decrement of 1.8W in C2 to an increment of 2.6W in C7, with negligible variation (less than 0.8W) for cases C3 to C6. Increasing the air temperature to 28°C produces a decrement on the Q_M of ~8W reaching the minimum Q_M of ~90W. When heat production cannot be further reduced, and the skin temperature is close to the upper limit, the proportion of latent heat dissipated needs to increase, as is observed in scenario C8. Using PRCS reduces the latent heat, and with the configuration SBS at 10°C, the heat balance is restored to the levels of an air temperature of 26°C and no PRCS. Finally, at 30°C of air temperature, the latent heat becomes more critical to maintain the heat balance. While PRCS improves sensible heat dissipation, the heat balance cannot reach comfort levels or equivalent temperatures of below 26°C.

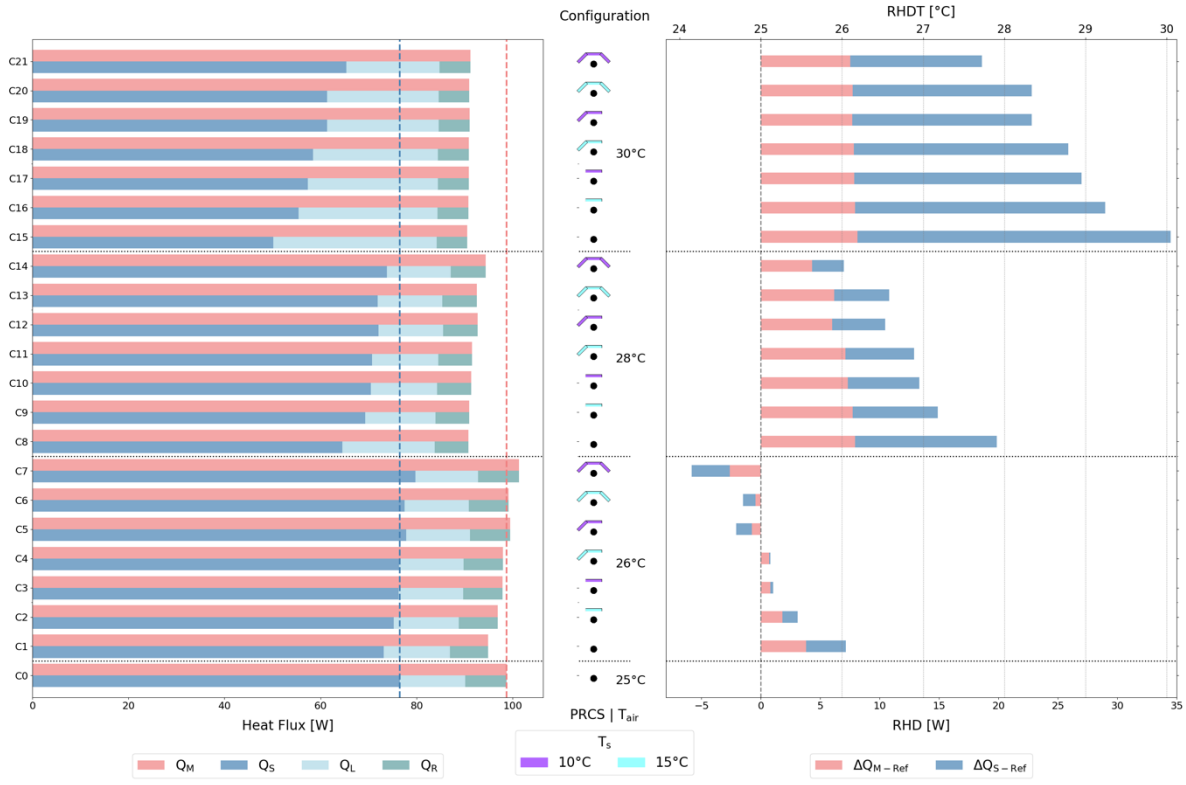

Figure 18. Impact of different PRCS on the human heat balance. On the **Left**: Metabolic heat produced (Q_M), Sensible heat losses through the skin (Q_S), Latent heat losses through the skin (Q_L), and heat loss through respiration (Q_R). On the **Right,** the change of the metabolic rate (MHD) and sensible

heat losses (SHD) relative to the baseline simulation, i.e., comfort (C0). In the **Middle** are indicated the configurations tested in each simulation. The PRCS configuration is represented by the icons: N ●, B ▬●, SB ◠●, and SBS ◠●◠; the PRCS surface temperature (Ts) is represented by the colour of the icon: 10°C (purple), 15°C (cyan); horizontal lines group the simulations at the same air temperature (Tair): C0 @ 25°C, C1-C7 @26°C, C8-C14@ 28°C, and C15-C21 @ 30°C. (For optimal interpretation, refer to the colour version of this figure). (Figure taken from [3])

Regarding the equivalent temperature proposed, RHDT, a linear relationship is found between the RHD for the reference simulations, i.e., without PRCS, and the indoor environment, in this case, characterised by the air temperature. In the reference scenarios, the MRT is equal to the air temperature, and the air velocity and RH remain constant across all the scenarios. Specifically, $RHDT = 0.1463 \times RHD + 25.001$ with $R = 0.99$. Accordingly, the use of the PRCS results in a RHDT in the range of 24°C – 25.5°C, 26°C – 27.1°C, and 27.8°C – 29.2°C, for an air temperature of 26°C, 28°C, and 30°C, respectively. On average, the PRCS SBS with a surface temperature of 10°C can lower the air's perceived temperature by ~2°C.

3.7 Design decisions

The exploratory and detailed comfort analysis revealed important characteristics of the impact of the PRCS on thermal comfort. For a more detailed description including further comfort metrics refer to [3]. In synthesis:

- At 26°C air temperature, a panel in the back with a surface temperature of 10°C can restore the thermoregulatory state exhibited in the reference scenario at 25°C air temperature. Under these conditions, all the evaluated metrics result within comfort ranges.
- At 28°C air temperature, without employing a PRCS system, the thermoregulatory system decreases the metabolic rate and increases the portion of heat dissipated by latent mechanisms. Utilising a panel with two side wings (configuration SBS) with a surface temperature of 10°C minimises latent heat dissipation and thus eliminates the risk of discomfort due to skin wettedness. In this scenario, the thermoregulatory state is equivalent to an air temperature of 26°C. However, the risk of discomfort due to radiant asymmetry becomes slightly noticeable, exceeding accepted limits. Using the panel with one side wing (SB) similarly affects the heat balance, reducing the risk of discomfort due to radiant asymmetry while accepting a slightly higher mean skin temperature.
- At 30°C air temperature, the most effective panel configuration, SBS with a surface temperature of 10°C, is necessary. While it cannot restore the thermoregulatory state to reference levels, it reduces skin wettedness by half and lowers the perceived air temperature by over 2°C. Nevertheless, the risk of discomfort due to radiant asymmetry needs further evaluation since it slightly exceeds the accepted limit.

With these points in mind, the panel design should be modular, allowing occupants to increase its effective area according to their preferences and needs, as well as the air temperature. Furthermore, the surface temperature should be maintained at around 10°C to ensure it has a significant impact not only at low but also at moderate air temperatures. This indicates that moisture condensation mitigation measures need to be considered when designing the PRCS.

4 Energy performance analysis

The second part of the simulation-aided design process of the decentralised, occupant-centric radiant cooling panel concerns the energy performance analysis. First, an exploratory cooling demand study is performed to identify the contexts where the proposed cooling solution has potential. Next, for the

contexts identified, the cooling performance of the cooling panels is estimated. This chapter presents the methods, modelling assumptions and results of this energy performance analysis.

4.1 Exploratory cooling demand analysis

The parameter three established in Section 2.4 considers different aspects that affect the indoor environment of the offices, exhibiting different cooling needs. As shown in Figure 19 (Left), a total set of 60 contexts are evaluated, resulting from varying the location, the size of the office, the occupancy level, and the building construction age.

This analysis is performed using building performance simulations with the simulation engine Energyplus v24.2.0 [54] and the simulation tool Cesar-P [55]. One key advantage of Cesar-P is its use of predefined building archetypes tailored for the Swiss context. The weather files correspond to typical meteorological year (TMY) data, derived from weather records collected between 2007 and 2021 for two locations: Fluntern, (Zürich) [56] and Lugano (Ticino) [57].

The office building is modelled as a single-story structure with a square footprint, representing two different office sizes: 100 m² (medium) and 400 m² (large). The roof and walls are connected to the outdoor environement. Occupant-related schedules, including occupancy, lighting use, and appliance use, follow the Swiss standard SIA 2024 [58]. Occupancy density is varied across three levels:

- Low density: 15 m² per person
- Medium density: 10 m² per person
- High density: 5 m² per person

For all scenarios, adiabatic ventilation is set at 2 air changes per hour (ACH) to occur only when there is occupancy, and the indoor temperature is high. This setup is designed to capture the effect of window opening, which naturally increases ventilation rates. Further, blinds are activated when solar radiation on the window exceeds 90 W/m².

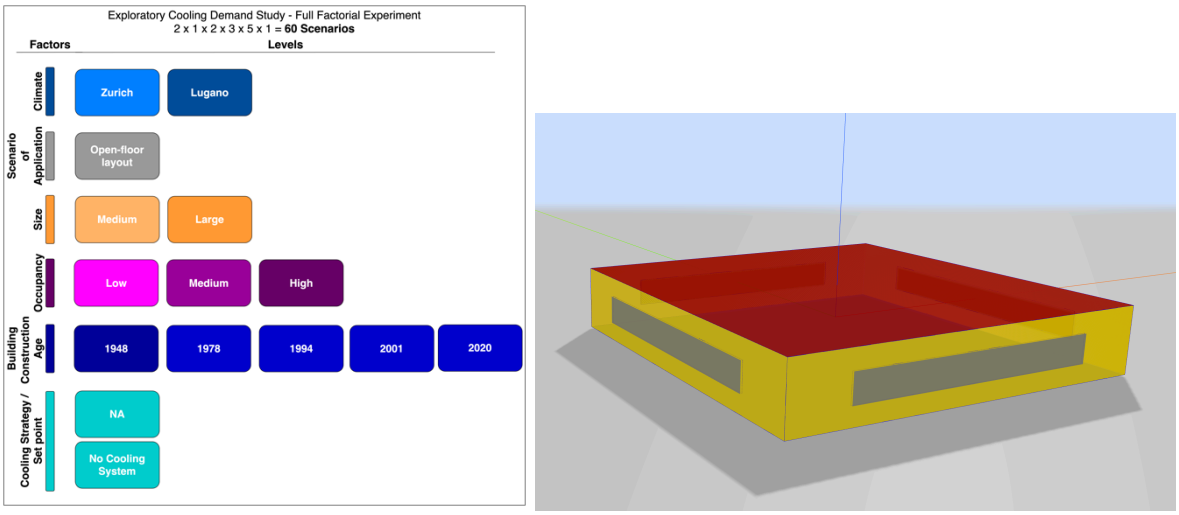

Figure 19. Exploratory cooling demand study – Parameters variation (Left); Generic building model (Right)

The construction age determines several key building parameters, including the nominal infiltration rate, window-to-wall ratio, and material properties of the walls, roof, floor, windows, and shading systems. These factors influence the nominal U-values of the building envelope, ensuring that each building scenario reflects realistic thermal performance. A detailed description of the building archetypes is available in [59] and the main parameters summarised in Table 8.

Table 8. Building archetypes characteristics (Created from [59])

Construction Year	Nominal U-Values				Mean	Infiltration-rate
	Walls	Windows	Floors	Roofs	WWR (%)	ACH (1/h)
≤ 1918	1.6	5.6	0.8	0.8	13	0.55
1919 - 1948	1.6	5.6	0.8	1.0	15	0.70
1949 - 1978	0.9	2.8	0.9	0.9	21	0.75
1979 - 1994	0.5	1.7	1.1	0.4	25	0.60
1995 - 2001	0.35	1.4	0.4	0.4	27	0.40
2002 - 2006	0.28	1.3	0.3	0.3	28	0.29
2007 - 2009	0.25	1.1	0.2	0.2	29	0.18
2010 - 2014	0.20	1.1	0.1	0.2	30	0.05
> 2014	0.15	0.0	0.1	0.1	30	0.05

Figure 20 presents a comparative analysis of the percentage of occupied hours within different temperature ranges across the 60 analysed scenarios. The temperature distribution follows a gradient, with lower temperatures (T < 26°C) expected to provide thermal comfort represented in light grey, slightly warm temperatures (26°C ≤ T < 27°C) in yellow, warmer temperatures (27°C ≤ T < 28°C) in orange, hot temperatures (28°C ≤ T < 29°C) in pink, and higher temperatures (T ≥ 29°C) depicted in dark red.

Location proves to be the most influential parameter; the percentage of hours during discomfort (T > 26°C) on average doubles when changing the location from Zurich (ZH) to Lugano (TI). Regarding building construction age, between 1948 and 1994, cooling performance increased due to improvements in construction materials, specifically lower U-values. After that period, there is a significant increase in the window-to-wall ratio, leading to higher solar gains and explaining the increase in hours at higher temperatures for buildings constructed in 2001 and 2020. Occupancy density and office size have a marginal influence on office overheating hours.

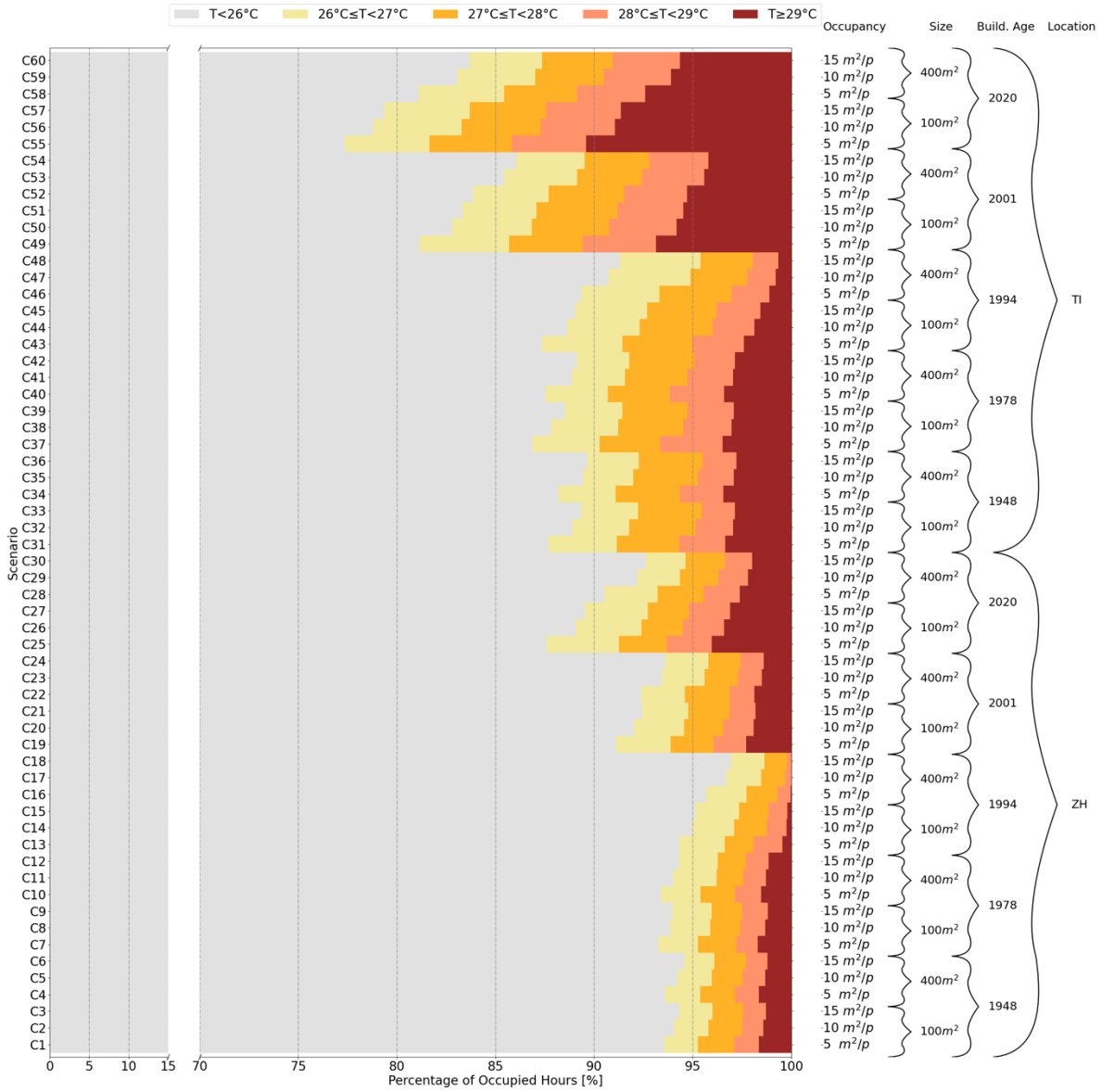

Figure 20. Distribution of temperature during occupancy.

Figure 21 zooms into the room temperature distribution when there is occupancy and the outdoor temperature is higher than 26°C, including the median. While this figure confirms that occupancy has a marginal influence, it shows that the size of the office has a significant influence for buildings constructed after 1994. In these cases, the smaller the office, the higher the median temperature. Furthermore, for buildings constructed between 1948 and 1994, the differences are small between Lugano and Zurich. In both locations, the median room temperature is between 26.5°C and 28.5°C. The difference lies in the range between minimum and maximum indoor temperatures, which is higher in Lugano than in Zurich. Finally, these results exclude seven scenarios from the study since their median temperature exceeds 30°C. This is because, as shown in Section 3.7, the radiant cooling panels have a limited effect at these temperature levels. These scenarios include small offices built in 2020 located in both Zurich and Lugano, and large offices with high occupancy built in 2020 located in Lugano.

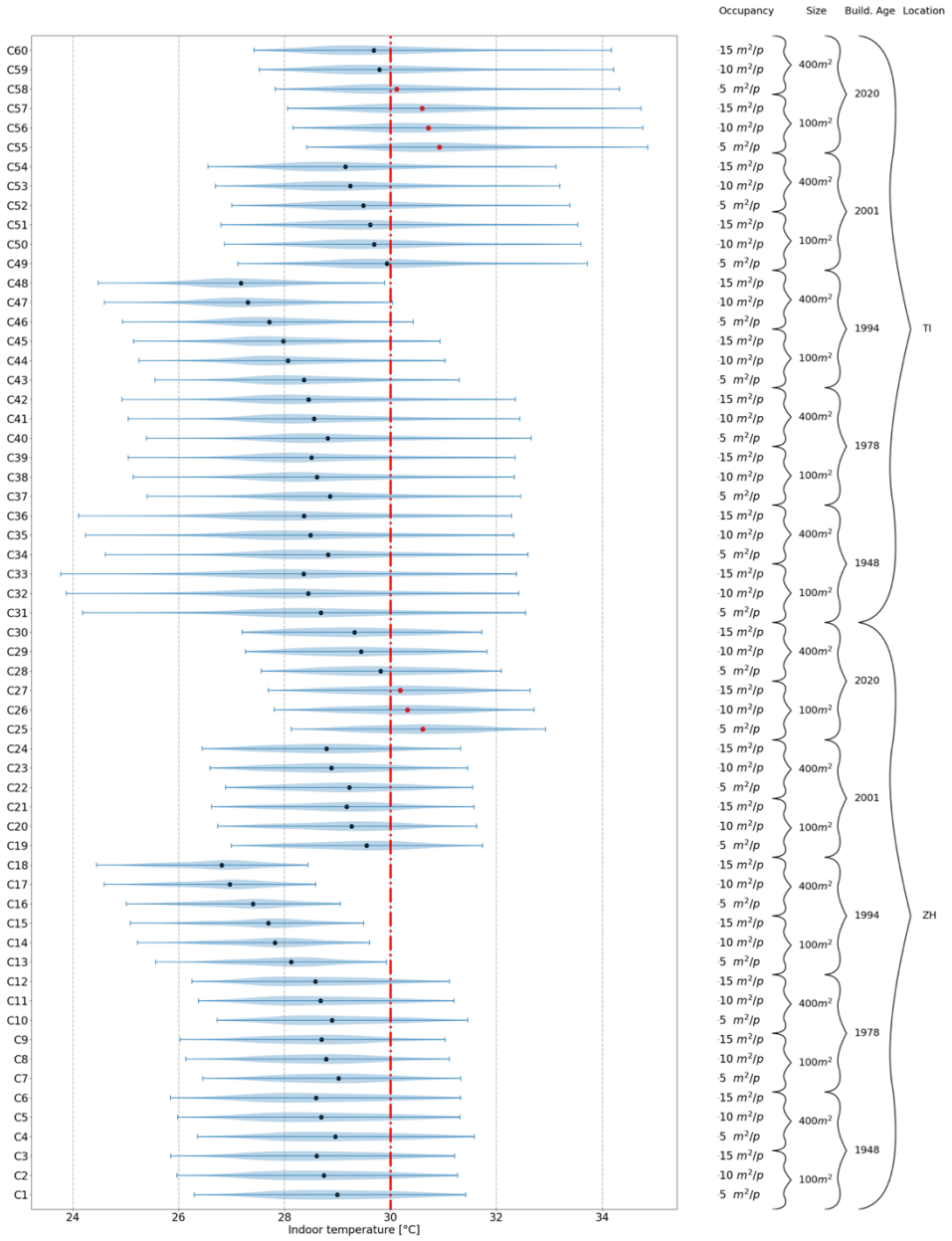

Figure 21. Distribution of temperature during occupancy and outdoor temperature larger than 26°C. (Figure adapted from [60])

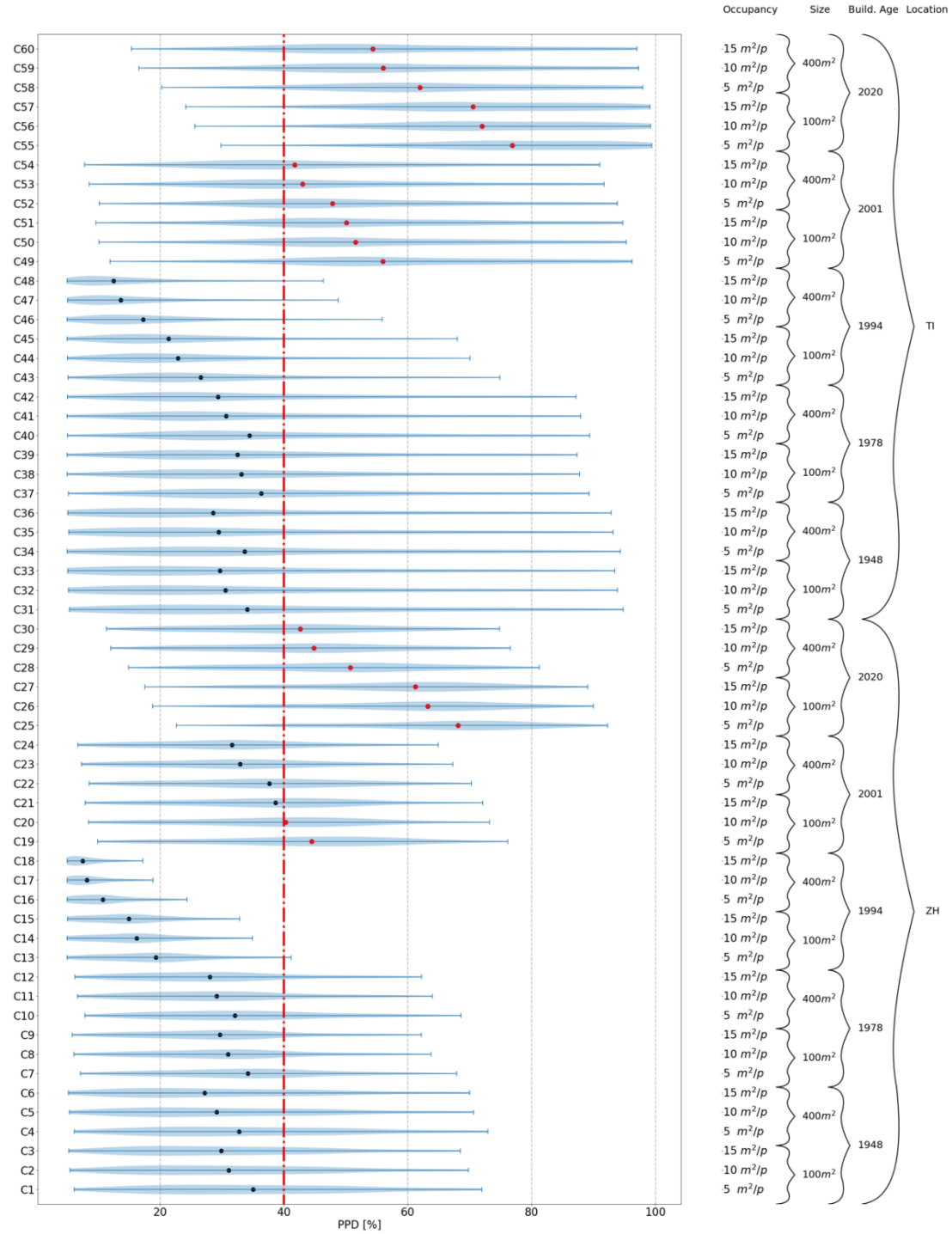

Figure 22. Distribution of PPD during occupancy and outdoor temperature larger than 26°C. (Figure adapted from [60])

Figure 22 explores the distribution of the percentage of people dissatisfied (PPD) during occupancy and outdoor temperatures higher than 26°C. It is noted that this is the most severe criterion for exclusion. Out of the 60 scenarios evaluated, 40 are identified as suitable for the proposed cooling solution to be implemented. All buildings constructed before 1994 display a PPD lower than 40%. While maximum values of approximately 75% in Zurich and 95% in Lugano are observed, they occur for a

reduced number of hours. Conversely, offices located in Zurich built in 2020, those with medium and high occupancy built in 2001, and all buildings located in Lugano built in 2020 present a PPD larger than 40%, indicating a need for different cooling solutions, such as fixed radiant cooling panels.

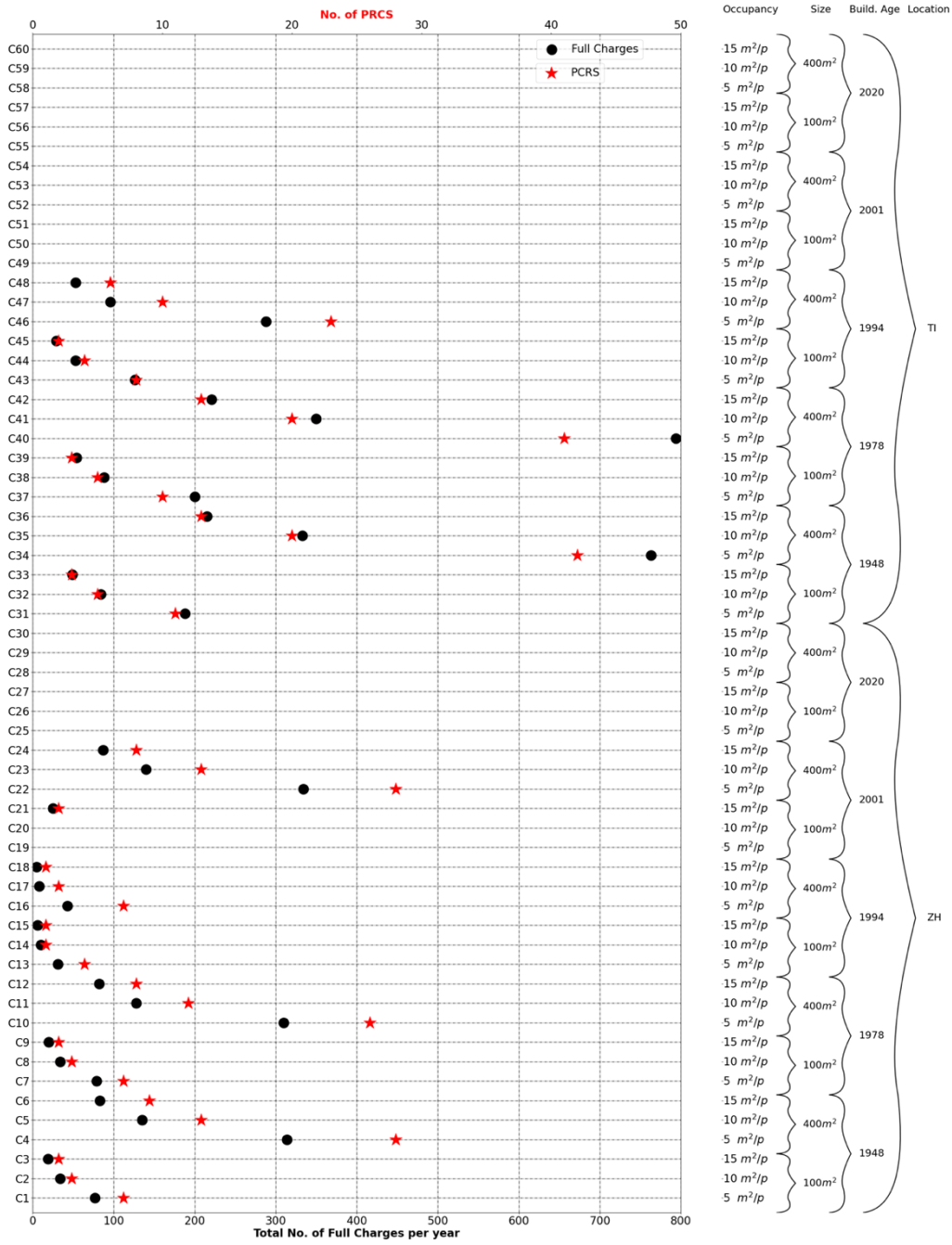

Figure 23. PRCS requirements (Figure adapted from [60])

4.2 PRCS requirements

Previously, 40 scenarios were identified for the potential deployment of the proposed radiant cooling solution using PRCS, considering temperature distribution and PPD. To estimate the number of PRCS units required and their charging operation, the following assumptions were made:

- The maximum allowable PPD is 10%.
- Once a PRCS is in use, it is only recharged at the end of the day.
- A PRCS with the SBS configuration is always used.

Based on these assumptions, the number of PRCS units and their total full charges were calculated and are presented in Figure 23. The results indicate that scenarios C34 and C40 have the highest requirements. These scenarios correspond to large offices with high occupancy density, located in Ticino and built between 1948 and 1978. In these cases, over 40 PRCS units are needed, with approximately 800 full charges per year.

Scenarios with high occupancy density, on average, require 20 PRCS units and around 400 full charges annually. For all other scenarios, the requirements are significantly lower—approximately 8 PRCS units and on average 100 full charges per year.

4.3 Energy storage and design decisions

To estimate the energy consumption of the system, key assumptions and design decisions must be made. According to the comfort analysis presented in Section 3.8, maintaining thermal comfort under the evaluated scenarios requires a radiant panel surface temperature of approximately 10°C. To achieve this, the PCM RT11HC from Rubitherm is selected, with a melting temperature range of 10–12°C [61].

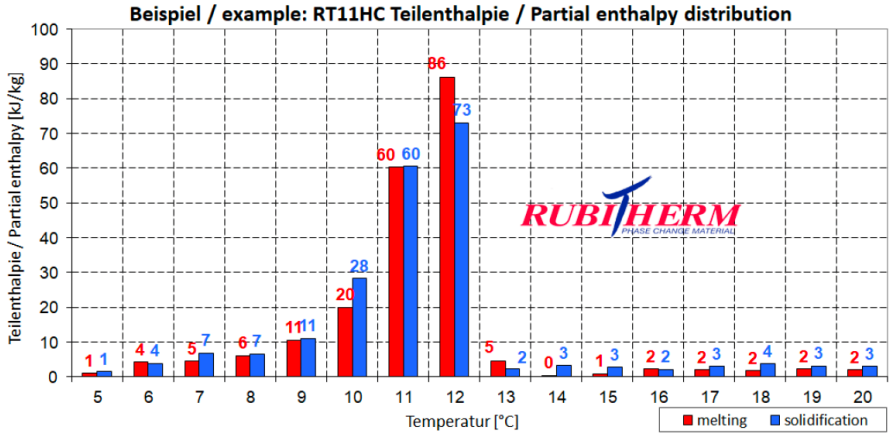

Figure 24. Partial enthalpy distribution - PCM RT11HC [61]

This PCM has a thermal storage capacity of 200 kJ/kg (55 Wh/kg) when operated between 20°C and 5°C, using conservative assumptions for charging and discharging temperatures. The PCM is macro-encapsulated in 450 mm × 300 mm × 15 mm aluminium casings.

To cover the required surface area, as analysed in Section 3.8, a total of 16 panels are needed. Each casing holds approximately 1 kg of PCM, resulting in a total PCM mass of 16 kg for the entire PRCS. Consequently, a full charge/discharge cycle of a single PRCS corresponds to the storage and release of 3200 kJ (approx. 880 Wh) of thermal energy. In Figure 25, this is translated into the total annual energy that is stored and discharged in the PRCS for each scenario using the number of full charges per year. Furthermore, a COP of 4 is assumed for the industrial fridge that charges the PRCS. Accordingly, the total annual electricity consumption is calculated.

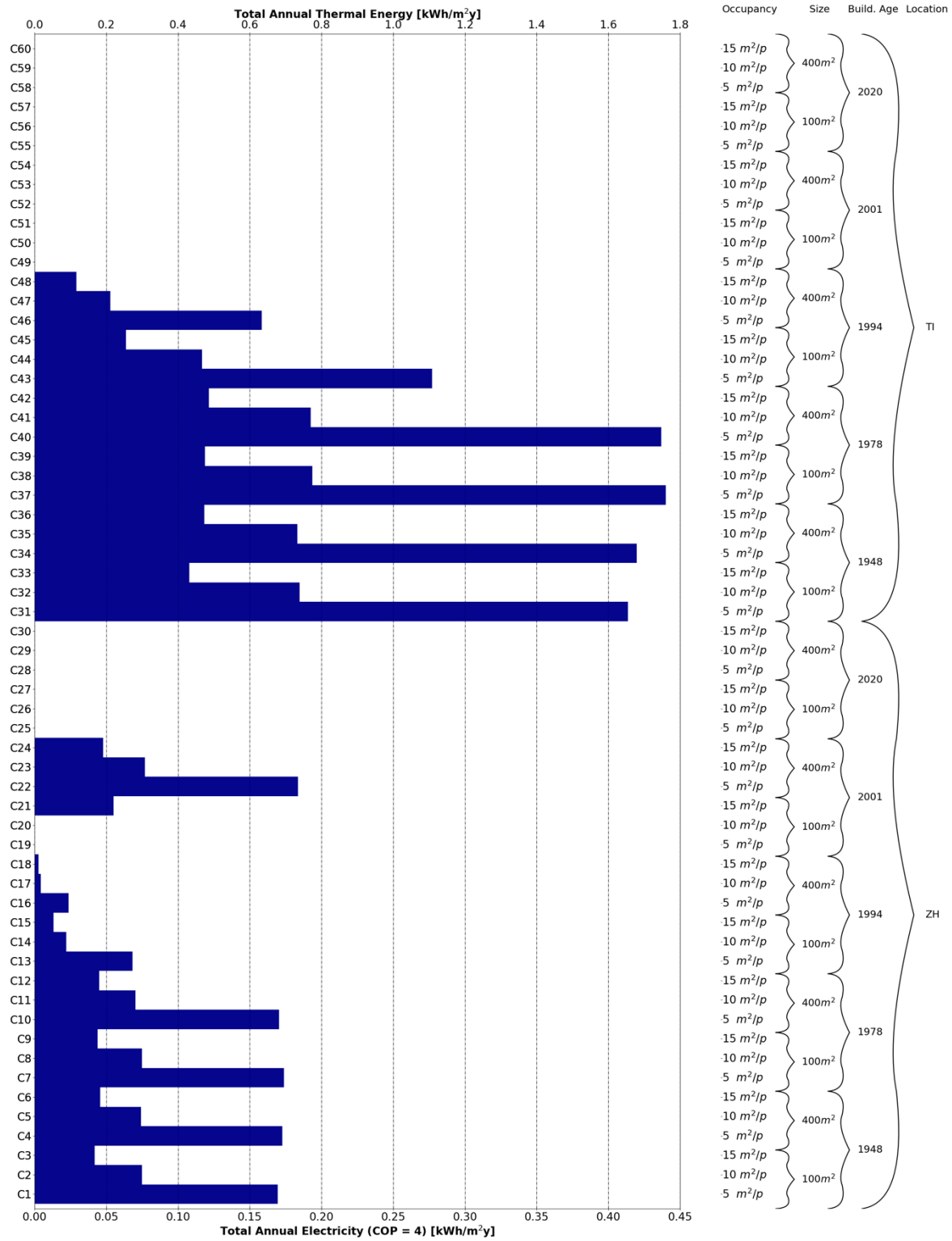

Figure 25. Thermal energy stored in the PRCS per year

5 Feasibility Analysis

This chapter describes the models and assumptions to quantify the proposed solution's potential. This feasibility analysis includes the estimation of energy savings for the scenarios identified in Section 4, and a high-level preliminary analysis of embodied emissions for the evaluation of environmental performance.

5.1 Energy savings

The building performance simulations used in Section 4 have been modified to quantify the energy-saving potential of the mobile radiant cooling solution. In these simulations, the room air is not conditioned by any mechanical system. Consequently, the indoor temperature is directly influenced by the energy balance between the indoor and outdoor environments, considering the envelope quality, internal heat gains, and the infiltration and ventilation rate, which is driven by indoor air quality rather than temperature.

To make fair comparisons that accounts for the thermal comfort level provided and the cooling load required, four scenarios are defined:

- PRCS: The cooling energy is calculated based on the number of PRCS units and the full charging/discharging cycles as defined in Section 4. It is acknowledged that occupants do not gain comfort levels for indoor temperatures above 28°C (see Section 3.7). However, discomfort is reduced by decreasing latent heat exchange, thereby reducing discomfort due to transpiration and sweat.
- HVAC @Teq: Instead of using PRCS to improve the thermal environment, an HVAC system represented by ideal loads is implemented. In this scenario, a variable cooling setpoint is calculated for each case. This setpoint is derived from the RHDT metric defined in Section 3.5 and quantified in Figure 18 (see Section 3.6.3). A relationship between indoor air temperature and heat balance using PRCS can be established to define an equivalent air temperature that produces the same impact on the heat balance as PRCS. In the studied case, this relationship is $RHDT = 0.91T_{indoor} + 0.41$. Accordingly, the indoor temperature calculated in Section 4 is corrected to the RHDT and defined as the cooling setpoint.
- PRCS + HVAC @T27°C: An HVAC system, represented by ideal cooling loads, is used in combination with PRCS. With a cooling setpoint of 27°C, occupants would perceive 25°C using PRCS, thus achieving the heat balance conditions of a neutral condition (see Section 3.6.1). The cooling load is then the sum of the load from the HVAC system and the load stored in PRCS.
- HVAC @25°C: Thermal comfort is achieved solely by an HVAC system with a cooling setpoint of 25°C.

Overall, Scenarios 1 and 2, as well as Scenarios 3 and 4, are equivalent in terms of the thermal comfort provided.

Figure 26 shows the cooling energy required by the 4 different scenarios proposed and applied to all the cases identified as suitable to deploy the PRCS (see Section 4.2). In general, the scenarios S1 and S3, where the PRCS are implemented, outperform scenarios S2 and S4, respectively. In average, S2 and S4 are six times larger than S1 and S3. Naturally, it is observed that the higher the occupancy density the lower the potential energy savings, i.e., with a minimum value of approximately 2 for the ratio S2:S1 or S4:S3.

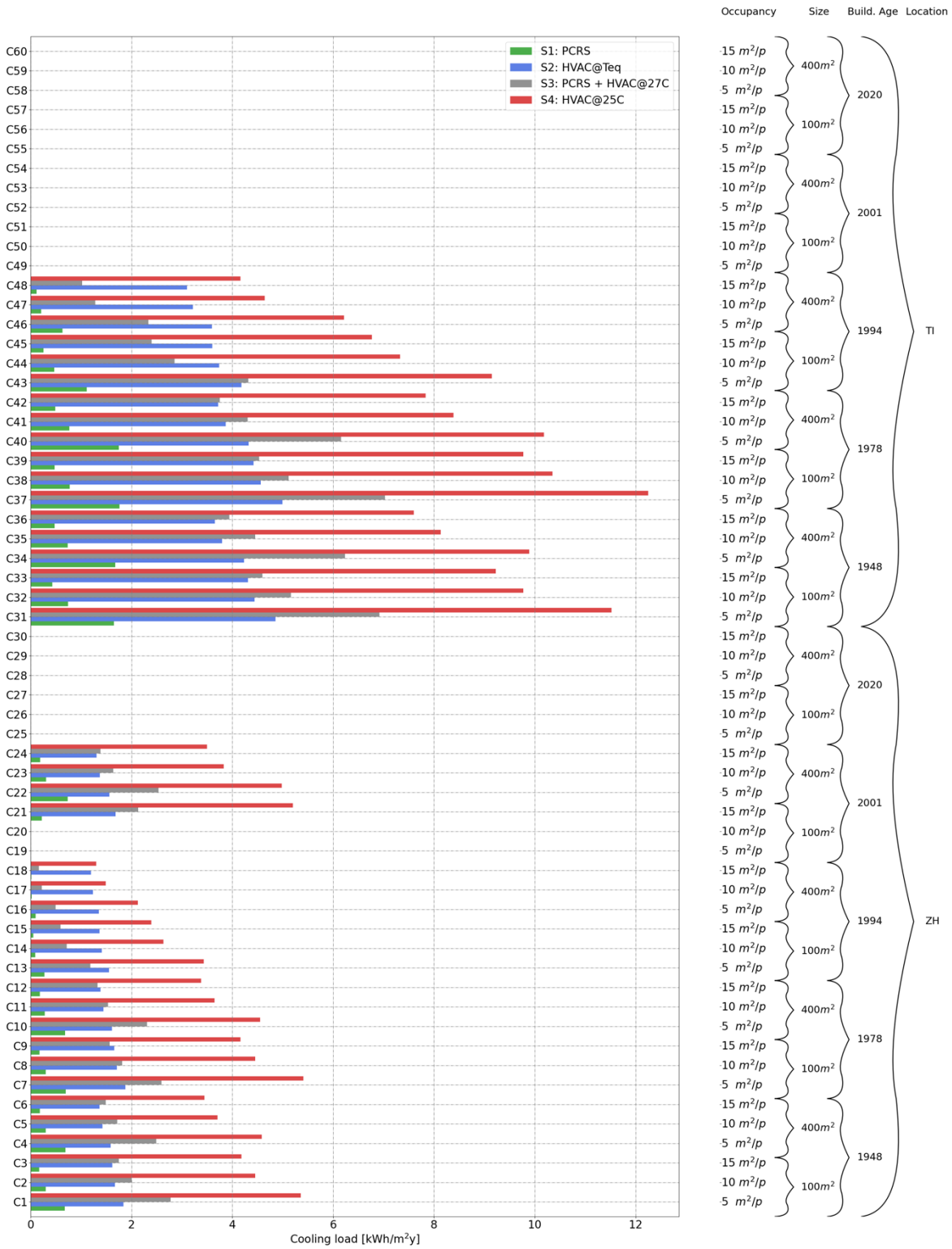

Figure 26. Cooling Loads - System Comparison (Figure adapted from [60])

The energy savings presented in this study are based on the cooling demand required to achieve equivalent thermal comfort across different scenarios, rather than on direct electricity consumption. While it is acknowledged that air conditioning systems typically operate with higher EERs, especially at higher evaporator temperatures (e.g., +18°C), the comparison here focuses on the reduction in total cooling demand due to the use of PRCS. The PRCS units operate intermittently, and target localized, occupant-level comfort, thereby reducing the need for full-space mechanical cooling. Although PRCS may have lower COP/EER values due to operating at lower temperatures (e.g., +5°C), the significantly shorter operating periods and smaller conditioned volumes lead to overall energy savings. Furthermore, thermal losses in the PRCS refrigeration units are recognized, but are relatively minor when compared to the reductions in the centralized HVAC cooling load.

5.2 Environmental performance

For the comparison between decentralized panel cooling and conventional cooling (reference), a specific selection for the reference system needs to be made. In order to allow for a fair comparison the following assumptions were made:

For all cases studied, a base ventilation rate of 2 ACH is ensured along with a control of the relative humidity in the room, in order to limit it to a maximum of 50%. This makes the different cases comparable and ensures that the relative humidity is controlled to the conditions under which the local panel cooling was investigated in detail by means of CFD simulations.

The following cases and conditions were set for the comparison.

- No conditioning: The simulation were run without temperature control (baseline)
- No conditioning with local panel cooling: Similar to baseline but with use of local panels to improve comfort. Energy demand is calculated in a post-processing step
- Partial temperature control with limited capacity: A conventional cooling system is assumed but with a limited capacity, such that the same comfort conditions can be achieved as with local panel cooling.
- Full temperature control: A conventional cooling system is assumed but without capacity limitations, such that the room temperature can be kept at 25°C.

Based on the presented cases and conditions for comparison a very rough and preliminary evaluation of embodied emissions is presented. The quantification is based on values taken from the KBOB list (https://www.kbob.admin.ch) for building energy systems. For the conventional cooling system, an activated ceiling was chosen as the cold emission system and two system variants were looked at for the cold generation. The variants are:

- Cold generation system assumed to be similar to the heat generation system with a specified capacity, expressed in W/m^2 cooled floor area.
- Cold generation system based on a water air heat pump of a selected capacity

To estimate the embodied emissions of the conventional cooling systems installed in the different building cases investigated, a classification is chosen based on a range of cooling loads. These include 20, 40 and 60 W/m2. The results for the embodied emissions are summarized in Table 9 and split into a best and a worst case. This differentiation stems from the different cold generation options that yields significant differences in the total embodied emissions.

Table 9. Estimate of embodied carbon emissions using values from KBOB for different assumptions for the reference cooling system, expressed as a best case and a worst case.

specific cooling load W/m2	20	40	60
	Case 1 – 100 m² office space		
total kg CO2_eq best case	750	922	1'093
total kg CO2_eq worst case	4'578	4'578	4'578
	Case 2 – 400 m² office space		
total kg CO2_eq best case	3'000	3'686	4'370
total kg CO2_eq worst case	6'312	10'312	14'312

For the comparison of the reference cooling system to the PRCS, two specific simulation cases are picked. These are cases, where the installed cooling capacity of an HVAC system producing the same thermal comfort as the PRCS corresponds to the specific cooling capacity ranges defined in Table 9. The first one is case C6 with a peak cooling load of 20 W/m2 and the second is case C32 with 40.8 W/m2. The peak cooling load is equal to the cooling capacity that needs to be installed. Both cases correspond to an office space built in 1948, assuming 400 m2 with an occupancy of 15 m2/occupant for C6 and 100 m2 with 10 m2/occupant for C32. C6 represents a case under the climate of Zurich, C32 the climate of Lugano.

To complement this, a preliminary estimate of operational emissions was added. Assuming a lifespan of 20 years, a COP of 5, and a Swiss electricity emission factor of 0.1 kg CO_2eq/kWh, annual electricity consumption and CO_2 emissions were calculated for the scenarios providing equivalent thermal comfort to the PRCS (HVAC@Teq; see Figure 26). For case C6 (20 W/m²), the operational emissions are 218 kg CO_2eq over 20 years; for case C32 (40.8 W/m²), they are 177 kg CO_2eq.

Now, regarding the PRCS, in C6, 9 units of panels in the SBS configuration (Table 4) are necessary, providing a cumulated cooling capacity of 7.92 kWh, while in C32 only 5 units are required with a cooling capacity of 4.4 kWh. This cooling capacity corresponds to the thermal energy storage capacity available from the phase change material. Besides the PCM, the macroencapsulation in aluminum needs to be considered and amounts to 50.4 kg in C6 and 28 kg in C32. The XPS frame used in the prototype panels is neglected in the preliminary calculation of the embodied emissions.

For being able to operate a PRCS a cooling system is needed to charge the PCM modules. For the selected cases C6 and C32 a large-scale professional fridge is selected. In Table 10, an estimate for the embodied emissions of the PRCS for the two cases is presented, considering the emissions from the macroencapsulated PCM on a paraffin basis of the product family RT from Rubitherm [62] together with the ones for a dedicated fridge [63]. This very coarse and preliminary analysis of the embodied emissions for the reference cooling system and the PRCS show that the latter presents a slim cooling solution, tailored to the specific needs which is also reflected in the 2-5 times lower embodied emissions when compared to a conventional cooling system.

Table 10. Estimate of embodied emissions of PRCS for two selected cases using macroencapsulated PCM on a paraffin basis.

	case 6 (400m2)	**case 32 (100m2)**
PCM (parafin)		
No of panels	9	5
storage capacity kWh	7.92	4.4
specific CO2 eq kg/kWh	46	
total CO2 eq kg	364.3	202.4
Aluminum for macroencapsulation		
amount of material kg	50.4	28
specific CO2 eq kg/kg	5.58	
total CO2 eq kg	281.2	156.2
Fridge for charging (large with hydro carbon refrigerant)		
CO2 eq emissions for a 250 litres fridge unit kg (cradle to gate)	237	
approx. required volume litres	900	500
total CO2 eq kg	853.2	474
No of panel charges / operating days of fridge	10	17
Electricity demand fridge kWh per lifetime (20 years)	440	416
CO2 intensity Swiss electricity grid kg CO2 eq / kWh	0.1	
Operational CO2 emissions	44.0	41.6
PRCS summed total CO2 eq kg	**1543**	**874**

5.3 Economical performance

To complement the environmental analysis, a simplified life cycle cost (LCC) assessment was conducted to estimate the annual cost of operating the PRCS on a per-panel basis. The total cost includes both capital expenditure (CAPEX) and operational expenditure (OPEX) over a 20-year assumed service life. Capital costs comprise the PCM modules, panel assembly, and a 5% allowance for miscellaneous materials. The annualized capital cost is derived using straight-line depreciation over the lifespan.

Operational costs include electricity consumption for recharging the panels and labour associated with panel handling. The electricity demand is based on the thermal capacity of each panel (0.88 kWh), the thermal efficiency of the cooling system (assumed 90%), and a COP of 4. Handling labour is estimated assuming 0.2 hours per charge and an average of 12 cycles per year, with staff costs at CHF 100/h. Energy costs are calculated using an electricity price of CHF 0.15/kWh.

The resulting total annual cost per panel is estimated at CHF 282.13, with the majority arising from labour for manual panel handling. This highlights a key opportunity for cost optimisation through process automation or integration into existing workflows.

Table 11. Estimate of total annual cost of PRCS

Capital cost				
		specific cost	total cost	
No of modules per panel	16	34	CHF	544.00
Panel design + material			CHF	250.00
subtotal			CHF	794.00
various materials 5%			CHF	39.70
total capital cost			**CHF**	**833.70**
life expectancy years	20	(unlimited no of cycles)		
annual capital cost			**CHF**	**41.69**
annual operational cost				
Energy capacity per panel kWh	0.88			
Fridge thermal efficiency	0.9			
COP of fridge	4			
Mean No of cycles per year	12			
Electricity demand per panel kWh	2.93			
Electricity price (CHF / kWh)		0.15	CHF	0.44
Handling time h per charging h	0.2			
Total handling time h	2.4			
Staff cost per h	CHF 100.00			
Panel handling cost			CHF	240.00
total annual operation cost			**CHF**	**240.44**
Total annual cost (CAPEX+OPEX)			**CHF**	**282.13**

6 Panel design and prototyping

The conclusions from the various workshops, along with the comfort, energy, and feasibility analyses, are integrated to define the PRCS system design. The PRCS needs to be modular to accommodate different requirements, such as active surface area and view factor. The unitary module of the system is illustrated in Figure 27. It consists of a thermal insulation panel made of extruded polystyrene rigid foam (XPS) with dimensions of 1250 x 500 x 60 mm. Embedded within the XPS panel are four aluminum casings filled with PCM RT11HC from the company Rubitherm. The PCM material has a melting temperature range of 10-12°C. This configuration controls the active side and reduces thermal losses.

Additionally, an attachable frame is designed to hold a thin plastic membrane to address potential condensation issues.

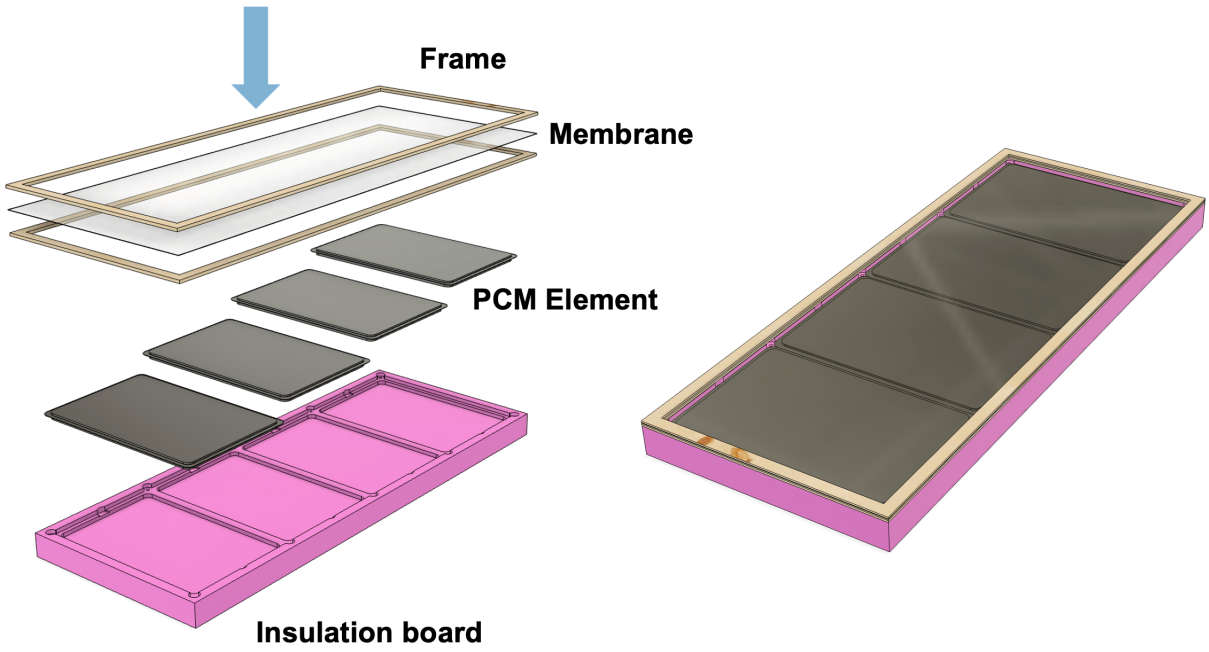

Figure 27. Modular panel design.

As shown in Figure 28, the XPS can be processed in a CNC to sculpt the PCM panels placements. This ensures a secure holding of the panels and eliminates the need for holders. It also allows the installation and exchange of unitary PCM panels on demand. Further, the module is tested to verify its functionality and dimensional tolerances

Workshop 3 – Prototype presentation

A final workshop was held with the industrial partner Witzig, to present the module's prototype, discuss possible enhancements, and explore possible integration into office spaces. Different applications such as integration to vertical or horizonal privacy panels were envisioned (see Figure 29). Figure 29, top). Possible limitations were identified regarding how easy and practical results interchanging single PCM panels. This is because, the final design, consist in 16 panels that need to be individually removed, recharged, and installed between operation. Nevertheless, the whole design was positively received.

The final and complete PRCS design, with one of the modules displaying the anti-condensation plastic cover is presented in Figure 29 (Bottom). With this design, the active surface area can vary from 0.62 m^2 to 2.5 m^2, depending on the needs. Further, a maximum of 880Wh of thermal energy can be stored.

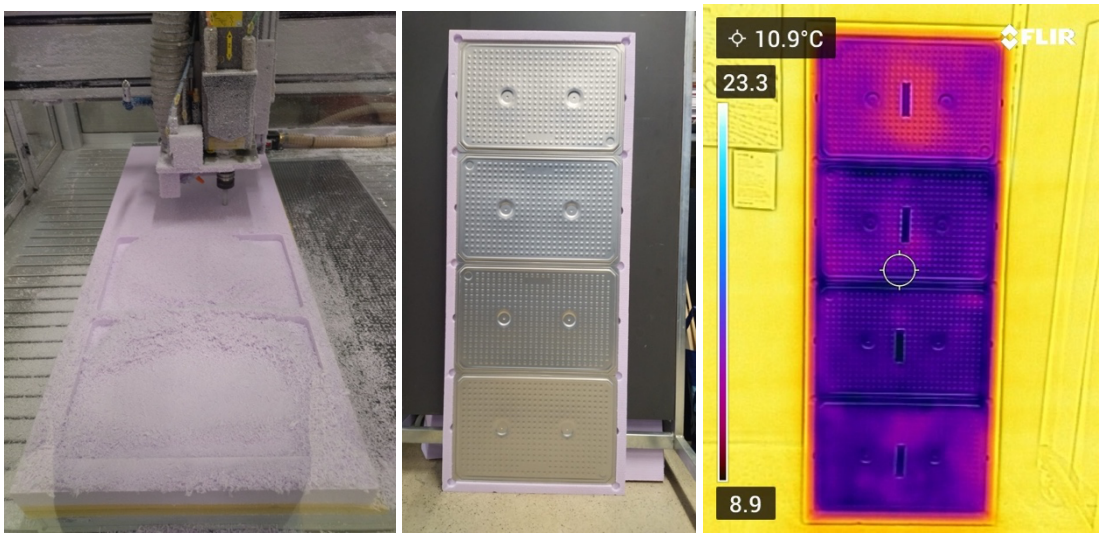

Figure 28. CNC processing of XPS (Left); Functional test (Right)

Figure 29. Prototype's presentation

7 Experimental testing

A high-level experimental campaign is conducted to have the first indications and impressions of the PRCS. They are tested with an experiment performed in a conditioned office. Two electrical heaters with a heating capacity of 2.4kW are installed to control the temperature of the room, ensuring air temperature ranges between 26°C and 29°C. The heaters are located behind shielding panels to prevent direct radiation on the subjects. A hygrostat-controlled evaporative humidifier with a capacity of 0.30l/h is installed to maintain the RH at approximately 50%. This is to ensure experimental conditions in the range of the simulations performed in Section 3. The PCM panels were refrigerated at 5.5°C for 12 hours to ensure all the material is solidified.

Figure 30. Experimental Setup

A humidity and temperature sensor SHT43 from the company Sensirion is installed to log the indoor conditions during the experimental campaign with a 5 min resolution. This sensor has an accuracy of 1.8 %RH and 0.48°C calibrated under the ISO/IEC 17025:2017 [64]. Further, a FLIR C5 thermal camera [65] is used to register the surface temperature of the subject and the PRCS. Figure 31 shows a snapshot of the temperature and relative humidity recorded during the tests.

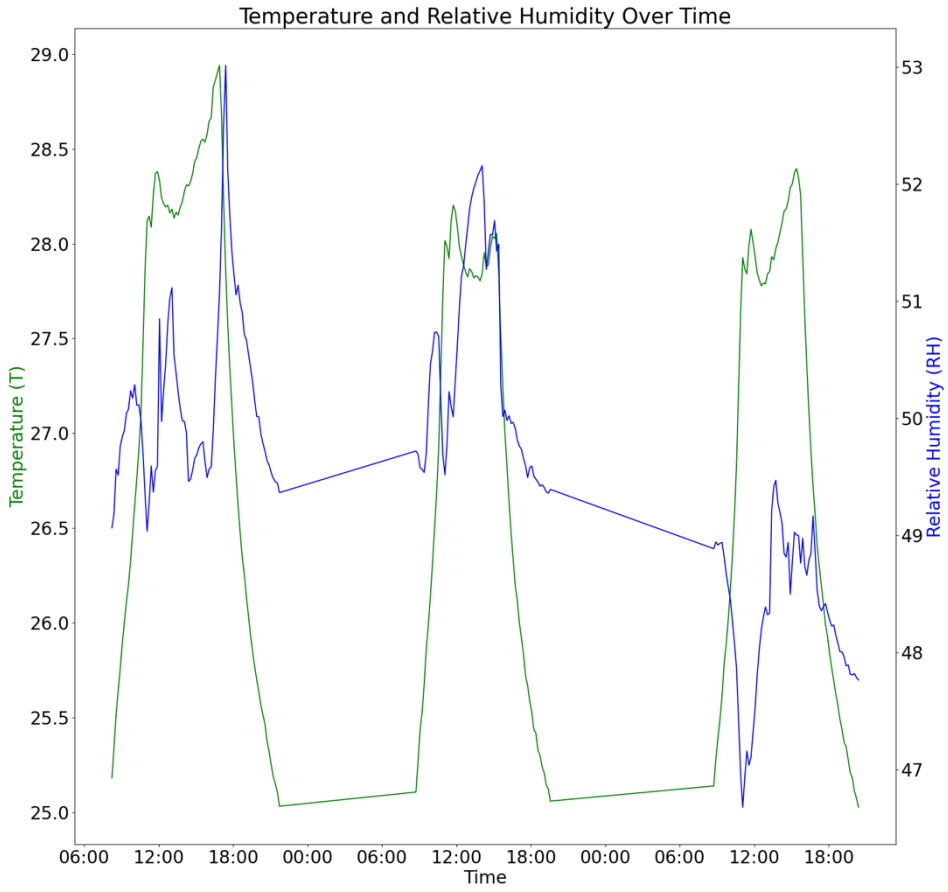

Figure 31. Indoor temperature and %RH during the experimental campaign.

Finally, along with the environmental parameters measured, a subjective evaluation is conducted. While this study is not statistically representative, the results give an idea of the impact of the PRCS on thermal perception. Based on the literature review presented in Section 2.1 and Table 1, a comfort survey is designed to understand the PRCS impact on global and local thermal comfort. The first section enquires about personal and contextual characteristics that influence thermal comfort, such as gender, age, activity performed before the test, and clothing level. In the second part, questions regarding global thermal perception, local sensation and possible sources of discomfort (if any) are formulated.

Six subjects (four males and two females) between 25 and 35 years old were interviewed. They were performing normal office activities sitting at a desk. They were asked to answer the questionnaire after 30 minutes of entering the room. This is to have a stabilisation and acclimatisation period. The tests were carried out at an average temperature of 28.1°C ±0.5°C.

Comfort Survey

Research Project MoCool
Institute for Building Technology and Process

DISCLAIMER: Your participation is entirely voluntary, and you may withdraw at any time without any consequences. The data collected will be processed anonymously to ensure your privacy and confidentiality. We will use the information gathered to test the design of radiant systems. Please be assured that all responses will be kept confidential and used solely for research purposes. If you have any questions or concerns about the study, feel free to contact our research team.

Section 1: General Information	
Age:	
Gender:	☐ Male ☐ Female ☐ Other ☐ Prefer not to say
Height:	
Weight:	
Date:	
Time:	
Activity Level in the last 15 minutes:	☐ Sedentary (sitting, typing) ☐ Light Activity (standing, walking slowly) ☐ Moderate Activity (walking briskly) ☐ High Activity (running, biking)

Which ensemble best matches what you are wearing right now?

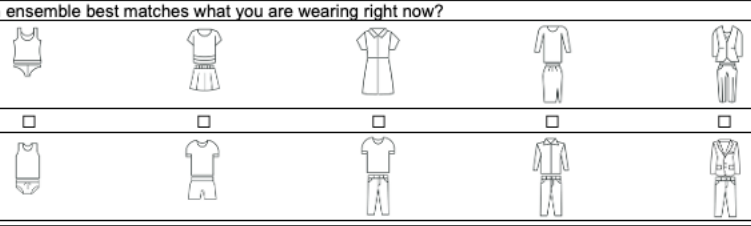

☐	☐	☐	☐	☐

Section 2:

How do you feel the temperature in this room right now?

	Cold	Cool	Slightly Cool	Neutral	Slightly Warm	Warm	Hot
	☐	☐	☐	☐	☐	☐	☐

How do you perceive the temperature in different parts of your body?

	Cold	Cool	Slightly Cool	Neutral	Slightly Warm	Warm	Hot
Head	☐	☐	☐	☐	☐	☐	☐
Chest	☐	☐	☐	☐	☐	☐	☐
Back	☐	☐	☐	☐	☐	☐	☐
Left Hand	☐	☐	☐	☐	☐	☐	☐
Right Hand	☐	☐	☐	☐	☐	☐	☐
Left Leg	☐	☐	☐	☐	☐	☐	☐
Right Leg	☐	☐	☐	☐	☐	☐	☐

How satisfied are you with the temperature?

	Very dissatisfied	Dissatisfied	Slightly dissatisfied	Neutral	Slightly satisfied	Satisfied	Very Satisfied
	☐	☐	☐	☐	☐	☐	☐

If you have expressed dissatisfaction with the temperature, how would you best describe the source (Check all that apply)

☐	Air is dry	☐	Room is to bright
☐	Air is humid	☐	Room is to dark
☐	Air is stuffy	☐	Uneven temperature (Front/Back)
☐	There are unsual odours	☐	Uneven temperature (Up/Down)
☐	Air movement to high	☐	Uneven temperature (Left/Right)
☐	Air movement to low	☐	Cold surrunding surfaces
☐	Drafts from windows	☐	Hot surrunding surfaces
☐	Othes. Please described:		

Figure 32. Comfort survey

Figure 33 presents a sample of thermographic images taken during the tests. A quasi-homogeneous distribution of temperature over the panels around the melting temperature, approximately. 10°C. The PRCS was tested with 16 PCM modules given the ranges of air temperature of around 28°C. During the entire experimental campaign, the PRCS remained under 12°C. In other words, they were not fully discharged.

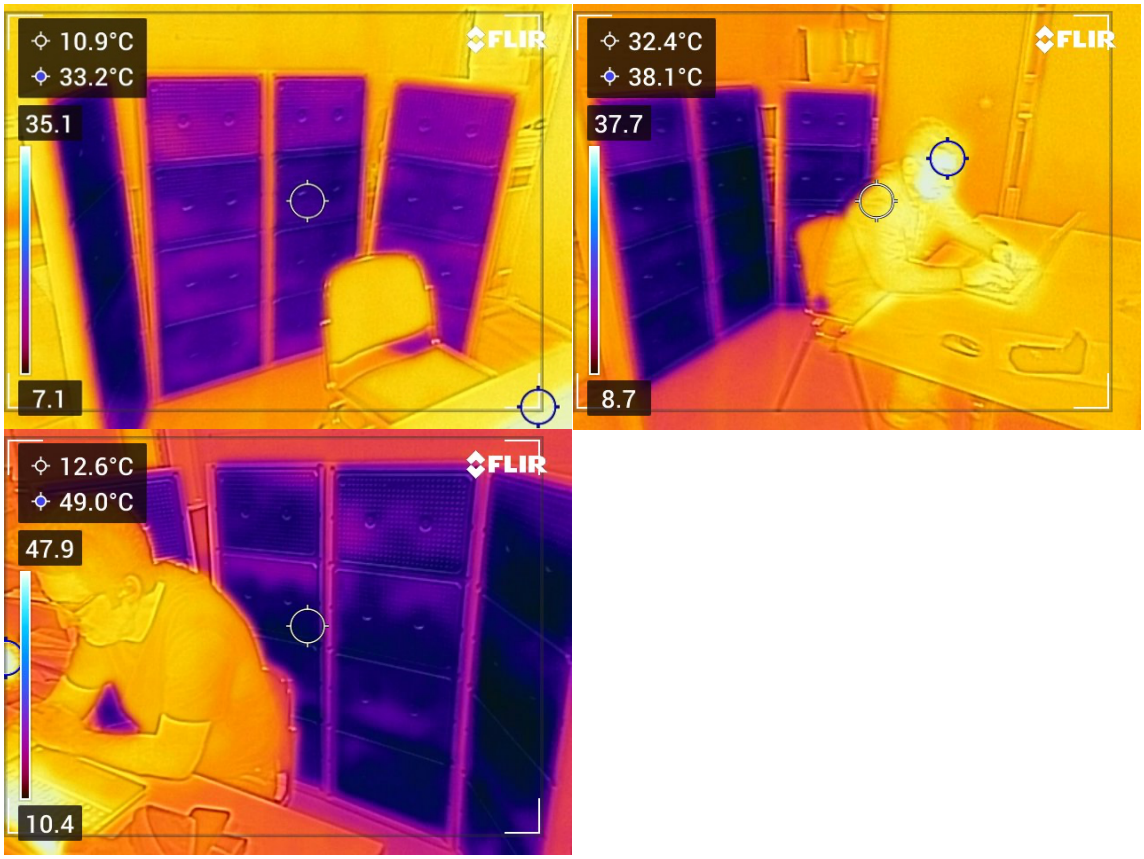

Figure 33. Thermographic images

It is important to highlight that this experiment is not considered statistically representative but indicates high-level characteristics of the system and indicates possible impacts and influences on thermal comfort. Accordingly, general observations are highlighted in this report:

- All the subjects were in a seated position, performing office activity on a laptop, and a clothing level between 0.5 and 0.7
- Most of the subjects reported a general slightly warm perception of the temperature of the room. Only one reported feeling warm and one feeling neutral
- Hands and legs followed the global perception, instead, there is an important variation between the head, chest and back. In general, the chest was perceived as warm and in discomfort. The back varied between neutral and slightly cool, and the head between neutral and slightly warm.
- The subjects' satisfaction with the temperature of the room varied between slightly dissatisfied (the majority) and neutral.
- The main sources of discomfort reported were related to the indoor air quality, e.g., air is stuffy and related to the temperature asymmetry between the chest and the back.
- With the indoor environmental quality of the room, no significant condensation was registered

While the tests showed that the PRCS was working as designed along with a positive indication of improving the thermal perception of the subjects, future work should include a more rigorous and statistically significative experimental campaign.

8 Conclusions and outlook

This study has explored the potential of decentralized, occupant-centric radiant cooling panels to enhance thermal comfort in office buildings during summer cooling conditions. Through a combination of simulations, prototyping, and experimental evaluations, several key findings have emerged. The implementation of mobile radiant cooling panels has demonstrated significant improvements in thermal comfort across various use cases and scenarios. These panels effectively address elevated temperatures, providing localized cooling that aligns with individual comfort preferences. Compared to traditional benchmark cooling systems, the mobile radiant cooling panels offer potential energy and embodied emission savings by reducing the reliance on full-space cooling.

Despite the promising outcomes, several limitations must be acknowledged. The steady-state CFD model used in this study does not account for dynamic and transient conditions. Additionally, latent loads and associated heat transfer mechanisms, such as respiration and sweating, are neglected, limiting the model's ability to assess condensation risks. The discretization of the human body in the thermoregulation model limits the assessment of local impacts on different body parts. Higher resolution models could provide more detailed insights, particularly for studying asymmetrical discomfort. The current implementation of the coupling scheme focuses on radiation heat exchange and skin temperature. To study environments with significant air temperature and velocity stratification, additional parameters such as air temperature, air velocity, and heat transfer coefficients need to be integrated.

The parametric sweep in the case study varied air temperature, PRCS configuration, and surface temperature. Future studies should consider additional parameters like air velocity, relative humidity, occupant distance from the PRCS, and activity and clothing levels. Moreover, the simplified room setup without windows, appliances, or furniture may overestimate the PRCS impact. While the thermoregulation model has been previously verified, fully validating the coupled thermoregulation-CFD model remains challenging due to the complexity of multi-physics interactions and the need for high-quality experimental data. Future work should focus on comprehensive verification, experimental validation, sensitivity analysis, and uncertainty quantification.

The findings of this study pave the way for several future research directions. Future work should incorporate dynamic and transient simulations to capture the temporal variations in indoor environments and their impact on thermal comfort. Incorporating latent loads into the CFD model will enable a more comprehensive assessment of factors such as relative humidity, skin and clothes moisture, and respiration on thermal comfort. Developing higher resolution thermoregulation models will enhance the understanding of local impacts on different body parts, particularly for asymmetrical discomfort studies.

Future studies should evaluate a broader range of parameters, including air velocity, relative humidity, occupant positioning, and activity levels. Additionally, incorporating elements like windows and furniture will provide a more realistic assessment of PRCS performance. A more extensive validation process, including experimental campaigns and sensitivity analyses, will improve the accuracy and applicability of the numerical framework across diverse conditions. Continued prototyping and real-world testing will provide valuable insights into the practical implementation of mobile radiant cooling panels. Gathering user feedback will further refine the design and functionality to meet occupant needs effectively.

9 Publications and other communications

J. Mahecha Zambrano and Luca Baldini, Integrating CFD and thermoregulation models: A novel framework for thermal comfort analysis of non-uniform indoor environments, Energy and Buildings, Volume 335, 2025, 115570, ISSN 0378-7788, https://doi.org/10.1016/j.enbuild.2025.115570. [3]

J. Mahecha Zambrano and Luca Baldini, Energy and thermal comfort performance of occupant-centric radiant cooling systems: Linking CFD, thermoregulation, and building performance simulations,

Journal of Physics: Conference Series, CISBAT 2025 - THE BUILT ENVIRONMENT IN TRANSITION, Submitted [60]

10 References

[1] T. Frank, 'Climate change impacts on building heating and cooling energy demand in Switzerland', *Energy Build.*, vol. 37, no. 11, pp. 1175–1185, Nov. 2005, doi: 10.1016/j.enbuild.2005.06.019.

[2] M. Berger and J. Worlitschek, 'The link between climate and thermal energy demand on national level: A case study on Switzerland', *Energy Build.*, vol. 202, p. 109372, Nov. 2019, doi: 10.1016/j.enbuild.2019.109372.

[3] J. Mahecha Zambrano and L. Baldini, 'Integrating CFD and thermoregulation models: A novel framework for thermal comfort analysis of non-uniform indoor environments', *Energy Build.*, p. 115570, Mar. 2025, doi: 10.1016/j.enbuild.2025.115570.

[4] D. Zhang, C. Li, and Z. Li, 'The application performance of individualized radiant cooling and heating systems, a review', *Build. Environ.*, vol. 256, p. 111488, May 2024, doi: 10.1016/j.buildenv.2024.111488.

[5] R. Garg, V. R. Khare, J. Mathur, and V. Garg, 'Performance Evaluation of Personalized Radiant Conditioning System for Cooling Mode', p. 8, 2017.

[6] H. Teufl, M. Schuss, and A. Mahdavi, 'Potential and challenges of a user-centric radiant cooling approach', *Energy Build.*, vol. 246, p. 111104, Sep. 2021, doi: 10.1016/j.enbuild.2021.111104.

[7] H. Teufl, M. Schuss, and A. Mahdavi, 'Laboratory tests of a prototypical user-centric radiant cooling solution', in *Journal of Physics: Conference Series*, IOP Publishing Ltd, Dec. 2021. doi: 10.1088/1742-6596/2069/1/012122.

[8] N. Li, D. He, Y. He, M. He, C. Song, and H. Chen, 'Experimental Study on Thermal Sensation of Radiant Cooling Workstation and Desktop Fan in Hot-humid Environment', *Procedia Eng.*, vol. 205, pp. 757–764, 2017, doi: 10.1016/j.proeng.2017.10.007.

[9] Y. He, 'Using radiant cooling desk for maintaining comfort in hot environment', *Energy Build.*, p. 11, 2017.

[10] R. Rawal, V. Garg, S. Kumar, and B. Adhvaryu, 'Evaluation of thermally activated furniture on thermal comfort and energy consumption: An experimental study', *Energy Build.*, vol. 223, p. 110154, Sep. 2020, doi: 10.1016/j.enbuild.2020.110154.

[11] N. Ismail and D. Ouahrani, 'Modelling of cooling radiant cubicle for an office room to test cooling performance, thermal comfort and energy savings in hot climates', *Energy*, vol. 244, Apr. 2022, doi: 10.1016/j.energy.2022.123185.

[12] N. Ismail and D. Ouahrani, 'A comprehensive optimization study of personal cooling radiant desks integrated to HVAC system for energy efficiency and thermal comfort in office buildings', *Int. J. Refrig.*, vol. 156, pp. 54–71, Dec. 2023, doi: 10.1016/j.ijrefrig.2023.09.023.

[13] Y. Liang and G. Huang, 'A Novel Low-Temperature Personalized Radiant Cooler: Thermal Environment and Local Thermal Comfort Evaluation', in *Proceedings of the 3rd International Civil Engineering and Architecture Conference*, vol. 389, M. Casini, Ed., in Lecture Notes in Civil Engineering, vol. 389. , Singapore: Springer Nature Singapore, 2024, pp. 491–500. doi: 10.1007/978-981-99-6368-3_41.

[14] Y. Liang, H. Wu, J. Yang, and G. Huang, 'Local thermal environment and thermal comfort of a novel low-temperature radiant structure using CFD simulation', *Energy Build.*, vol. 308, p. 114007, Apr. 2024, doi: 10.1016/j.enbuild.2024.114007.

[15] V. R. Khare, R. Garg, J. Mathur, and V. Garg, 'Thermal Comfort Analysis of Personalized Conditioning System and Performance Assessment with Different Radiant Cooling Systems', *Energy Built Environ.*, vol. 4, no. 1, pp. 111–121, Feb. 2023, doi: 10.1016/j.enbenv.2021.09.001.

[16] W. Zhao, S. Kilpeläinen, R. Kosonen, and J. Jokisalo, 'Experimental comparison of local low velocity unit combined with radiant panel and diffuse ceiling ventilation systems', *Indoor Built Environ.*, vol. 29, no. 6, pp. 895–914, Jul. 2020, doi: 10.1177/1420326X20918398.

[17] N. Ismail, ‘A comprehensive optimization study of personal cooling radiant desks integrated to HVAC system for energy efficiency and thermal comfort in office buildings’, *Int. J. Refrig.*, 2023.
[18] M. Kimmling and S. Hoffmann, ‘Preliminary study of thermal comfort in buildings with PV-powered thermoelectric surfaces for radiative cooling’, *Energy Procedia*, vol. 121, pp. 87–94, Sep. 2017, doi: 10.1016/j.egypro.2017.07.484.
[19] A. H. Osman, M. Artus, H. Alsaad, C. Koch, and C. Voelker, ‘Assessing a thermoelectric radiative cooling partition as a personalised comfort system using empirical experiments enhanced by digital shadow visualisation’, *Build. Environ.*, vol. 245, p. 110833, Nov. 2023, doi: 10.1016/j.buildenv.2023.110833.
[20] R. Rawal, V. Garg, S. Kumar, and B. Adhyaru, ‘Impact Of Thermally Activated Furniture System On Thermal Comfort’, Rome, Italy, 2019, pp. 2531–2539. doi: 10.26868/25222708.2019.210907.
[21] E. Teitelbaum *et al.*, ‘Membrane-assisted radiant cooling for expanding thermal comfort zones globally without air conditioning’, *Proc. Natl. Acad. Sci.*, vol. 117, no. 35, pp. 21162–21169, Sep. 2020, doi: 10.1073/pnas.2001678117.
[22] J. Kuht and A. D. Farmery, ‘Body temperature and its regulation’, *Anaesth. Intensive Care Med.*, vol. 22, no. 10, pp. 657–662, Oct. 2021, doi: 10.1016/j.mpaic.2021.07.004.
[23] B. R. Kingma, A. J. Frijns, L. Schellen, and W. D. van Marken Lichtenbelt, ‘Beyond the classic thermoneutral zone: Including thermal comfort’, *Temperature*, vol. 1, no. 2, pp. 142–149, Sep. 2014, doi: 10.4161/temp.29702.
[24] Z. J. Schlader, ‘The human thermoneutral and thermal comfort zones: Thermal comfort in your own skin blood flow’, *Temperature*, vol. 2, no. 1, pp. 47–48, Mar. 2015, doi: 10.4161/23328940.2014.983010.
[25] M. K. Chithramol and S. R. Shine, ‘Review on modelling approaches of thermoregulation mechanisms’, *J. Therm. Anal. Calorim.*, vol. 148, no. 17, pp. 9343–9360, Sep. 2023, doi: 10.1007/s10973-023-12132-1.
[26] A. C. Burton, ‘The Application of the Theory of Heat Flow to the Study of Energy Metabolism: Five Figures’, *J. Nutr.*, vol. 7, no. 5, pp. 497–533, May 1934, doi: 10.1093/jn/7.5.497.
[27] W. Machle and T. F. Hatch, ‘Heat: man’s exchanges and physiological responses’, *Physiol. Rev.*, vol. 27, no. 2, pp. 200–227, Apr. 1947, doi: 10.1152/physrev.1947.27.2.200.
[28] H. H. Pennes, ‘Analysis of Tissue and Arterial Blood Temperatures in the Resting Human Forearm’, *J. Appl. Physiol.*, vol. 1, no. 2, pp. 93–122, Aug. 1948, doi: 10.1152/jappl.1948.1.2.93.
[29] E. H. Wissler, ‘A mathematical model of the human thermal system’, *Bull. Math. Biophys.*, vol. 26, no. 2, pp. 147–166, Jun. 1964, doi: 10.1007/BF02476835.
[30] R. J. Crosbie, J. D. Hardy, and E. Fessenden, ‘Electrical Analog Simulation of Temperature Regulation in Man’, *IRE Trans. Bio-Med. Electron.*, vol. 8, no. 4, pp. 245–252, Oct. 1961, doi: 10.1109/TBMEL.1961.4322924.
[31] J. A. J. Stolwijk, ‘A mathematical model of physiological temperature regulation in man’, NASA-Langley, 1971.
[32] J. Werner, ‘Mathematical Simulation of the Human Thermal System’, in *Advanced Simulation in Biomedicine*, D. P. F. Möller, Ed., New York, NY: Springer, 1990, pp. 141–171. doi: 10.1007/978-1-4419-8614-6_7.
[33] D. Fiala, K. J. Lomas, and M. Stohrer, ‘A computer model of human thermoregulation for a wide range of environmental conditions: the passive system’, *J. Appl. Physiol.*, vol. 87, no. 5, pp. 1957–1972, Nov. 1999, doi: 10.1152/jappl.1999.87.5.1957.
[34] X. Xu and J. Werner, ‘A Dynamic Model of the Human/Clothing/Environment-System’, *Appl. Human Sci.*, vol. 16, no. 2, pp. 61–75, 1997, doi: 10.2114/jpa.16.61.
[35] X. Xu, P. Tikuisis, R. Gonzalez, and G. Giesbrecht, ‘Thermoregulatory model for prediction of long-term cold exposure’, *Comput. Biol. Med.*, vol. 35, no. 4, pp. 287–298, May 2005, doi: 10.1016/j.compbiomed.2004.01.004.
[36] Y. Takahashi *et al.*, ‘Thermoregulation model JOS-3 with new open source code’, *Energy Build.*, vol. 231, p. 110575, Jan. 2021, doi: 10.1016/j.enbuild.2020.110575.
[37] OpenCFD Ltd, ‘OpenFOAM v2306’. 2023. [Online]. Available: https://doc.openfoam.com/2306/
[38] *OpenFOAM*. ESI OpenCFD. [Online]. Available: https://www.openfoam.com/news/main-news/openfoam-v2312

[39] Uekermann, Benjamin *et al.*, 'preCICE v2: A sustainable and user-friendly coupling library [version 2; peer review: 2 approved]', 2022, doi: 10.12688/openreseurope.14445.2.
[40] G. Chourdakis, D. Schneider, and B. Uekermann, 'OpenFOAM-preCICE: Coupling OpenFOAM with External Solvers for Multi-Physics Simulations', *OpenFOAM® J.*, vol. 3, pp. 1–25, Feb. 2023, doi: 10.51560/ofj.v3.88.
[41] M. La Gennusa, A. Nucara, G. Rizzo, and G. Scaccianoce, 'The calculation of the mean radiant temperature of a subject exposed to the solar radiation—a generalised algorithm', *Build. Environ.*, vol. 40, no. 3, pp. 367–375, Mar. 2005, doi: 10.1016/j.buildenv.2004.06.019.
[42] Q. Zhao, Z. Lian, and D. Lai, 'Thermal comfort models and their developments: A review', *Energy Built Environ.*, vol. 2, no. 1, pp. 21–33, Jan. 2021, doi: 10.1016/j.enbenv.2020.05.007.
[43] J. Van Hoof, 'Forty years of Fanger's model of thermal comfort: comfort for all?', *Indoor Air*, vol. 18, no. 3, pp. 182–201, Jun. 2008, doi: 10.1111/j.1600-0668.2007.00516.x.
[44] J. Zhao *et al.*, 'From characteristics to practical applications of skin temperature in thermal comfort research – A comprehensive review', *Build. Environ.*, vol. 262, p. 111820, Aug. 2024, doi: 10.1016/j.buildenv.2024.111820.
[45] J. Liu and C. Yang, 'A modified method of the standard effective temperature (SET) based on the extended mean skin temperature index (EMSTI)', *Energy Build.*, vol. 279, p. 112682, Jan. 2023, doi: 10.1016/j.enbuild.2022.112682.
[46] H. Sokolová and A. Psikuta, 'Using a human thermoregulation model as a tool for design and refurbishment of industrial spaces for human occupancy', *Energy Build.*, vol. 168, pp. 76–85, Jun. 2018, doi: 10.1016/j.enbuild.2018.03.014.
[47] M. Beyer, L. Schinke, G. Alessio, J. Seifert, and M. De Carli, 'Investigations of (local) thermal comfort as a function of radiation asymmetry and vertical air temperature difference', *E3S Web Conf.*, vol. 111, p. 02053, 2019, doi: 10.1051/e3sconf/201911102053.
[48] X. Su, Y. Yuan, Z. Wang, W. Liu, L. Lan, and Z. Lian, 'Human thermal comfort in non-uniform thermal environments: A review', *Energy Built Environ.*, vol. 5, no. 6, pp. 853–862, Dec. 2024, doi: 10.1016/j.enbenv.2023.06.012.
[49] I. Malcevic, 'Sitting Mannequin'. GrabCAD, https://grabcad.com/library/sitting_mannequin-1, 2020.
[50] M. Charlton *et al.*, 'The effect of constitutive pigmentation on the measured emissivity of human skin.', *PloS One*, vol. 15, no. 11, p. e0241843, 2020, doi: 10.1371/journal.pone.0241843.
[51] H. Zhang, T. L. Hu, and J. Ch. Zhang, 'Surface emissivity of fabric in the 8–14 μ m waveband', *J. Text. Inst.*, vol. 100, no. 1, pp. 90–94, Mar. 2009, doi: 10.1080/00405000701692486.
[52] J. Mahecha Zambrano and L. Baldini, 'Interim Report - MoCOOL – Occupant-centric, mobile, radiant panel cooling for increasing summer comfort in offices', Zurich University of Applied Sciences, Publisher Swiss Federal Office of Energy SFOE contract number: SI/502568-01, 2023. Accessed: Jul. 02, 2024. [Online]. Available: https://www.aramis.admin.ch/Texte/?ProjectID=51654
[53] M. Andrés-Chicote, A. Tejero-González, E. Velasco-Gómez, and F. J. Rey-Martínez, 'Experimental study on the cooling capacity of a radiant cooled ceiling system', *Energy Build.*, vol. 54, pp. 207–214, Nov. 2012, doi: 10.1016/j.enbuild.2012.07.043.
[54] EnergyPlus™, *EnergyPlus*. (2025). [Online]. Available: https://energyplus.net/
[55] K. Orehounig, L. Fierz, J. Allan, S. Eggimann, N. Vulic, and A. Bojarski, 'CESAR-P: A dynamic urban building energy simulation tool', *J. Open Source Softw.*, vol. 7, no. 78, p. 4261, Oct. 2022, doi: 10.21105/joss.04261.
[56] Climate.OneBuilding.Org, 'CHE_ZH_Zurich.Fluntern.066600_TMYx.2007-2021.epw'. 2024. [Ewp]. Available: https://climate.onebuilding.org/
[57] Climate.OneBuilding.Org, 'CHE_TI_Lugano.067700_TMYx.2007-2021.epw'. 2024. [Ewp]. Available: https://climate.onebuilding.org/
[58] SIA, *Standard-Nutzungsbedingungen für die Energie-und Gebbäude-technik*, 2006, 2024.
[59] D. Wang, J. Landolt, G. Mavromatidis, K. Orehounig, and J. Carmeliet, 'CESAR: A bottom-up building stock modelling tool for Switzerland to address sustainable energy transformation strategies', *Energy Build.*, vol. 169, pp. 9–26, Jun. 2018, doi: 10.1016/j.enbuild.2018.03.020.
[60] J. Mahecha Zambrano and L. Baldini, 'Energy and thermal comfort performance of occupant-centric radiant cooling systems: Linking CFD, thermoregulation, and building performance

simulations', presented at the CISBAT 2025 - THE BUILT ENVIRONMENT IN TRANSITION, Journal of Physics: Conference Series, 2025. [Online]. Available: Submitted
[61] Rubitherm Technologies GmbH, 'Data sheet - RT11HC'. 2022. [Online]. Available: https://www.rubitherm.eu/media/products/datasheets/Techdata_-RT11HC_EN_08102020.PDF
[62] R. Hischier, F. Reale, V. Castellani, and S. Sala, 'Environmental impacts of household appliances in Europe and scenarios for their impact reduction', *J. Clean. Prod.*, vol. 267, p. 121952, Sep. 2020, doi: 10.1016/j.jclepro.2020.121952.
[63] A. Legrain, E. Sv-Do, and J. Maurer, 'Carbon footprint analysis of SV faculty refrigeration equipment'.
[64] Sensirion, 'Specifications - Datasheet: SHT43', 2024. [Online]. Available: https://sensirion.com/products/catalog/SHT43
[65] Flir, 'Flir C5 - Thermal camera'. [Online]. Available: https://www.flir.eu/products/c5/?vertical=condition%20monitoring&segment=solutions